Preconditioning immersed isogeometric finite element methods with application to flow problems

Preconditioning immersed isogeometric finite element methods with application to flow problems

F. de Prenter[a,*], C.V. Verhoosel[a], E.H. van Brummelen[a]

[a]*Department of Mechanical Engineering, Eindhoven University of Technology, The Netherlands*

Abstract

Immersed finite element methods generally suffer from conditioning problems when cut elements intersect the physical domain only on a small fraction of their volume. We present a dedicated Additive-Schwarz preconditioner that targets the underlying mechanism causing the ill-conditioning of these methods. This preconditioner is applicable to problems that are not symmetric positive definite and to mixed problems. We provide a motivation for the construction of the Additive-Schwarz preconditioner, and present a detailed numerical investigation into the effectiveness of the preconditioner for a range of mesh sizes, isogeometric discretization orders, and partial differential equations, among which the Navier-Stokes equations.

Keywords: Immersed finite element method, Fictitious domain method, Navier-Stokes, Iterative solver, Condition number, Preconditioning

1. Introduction

Immersed or unfitted finite element methods have been demonstrated to have great potential for problems that are posed on domains for which traditional mesh-fitting techniques encounter problems, such as prohibitively large meshing costs or the necessity for manual intervention. In recent years, immersed methods – such as the finite cell method [1], CutFEM [2] and immersogeometric analysis [3] – have been a valuable companion to isogeometric analysis [4] as they enable computations on volumetric domains based on the availability of merely a CAD surface representation [5, 6] or voxelized geometries [7]. Additionally, immersed techniques can be considered as a natural way to incorporate CAD trimming curves in the design-through-analysis cycle [8–11]. Flow problems on immersed grids have been studied for decades, see e.g., the pioneering work in [12, 13] and the more recent review article [14]. Contemporary work on immersed flow problems involves numerous applications, such as: flows around complex (CAD) objects [15–17]; fluid-structure interaction with large deformations [18–24]; multiphase flows [25]; topology optimization [26] and flow problems on scanned domains such as, e.g., imbibition into porous media or biomechanical applications [3, 27, 28].

A disadvantage of immersed finite element methods is that they can result in severely ill-conditioned matrices when the system contains elements that only intersect the physical domain on a small fraction of their volume, see e.g., [7, 8, 19, 29–35]. Ill-conditioning caused by small volume fractions is not exclusive to immersed finite element methods, and also occurs in the extended or generalized finite element method (XFEM/GFEM) [36–41] and in the immersed finite volume method [42].

Multiple techniques exist to resolve the conditioning problems of immersed finite element methods. A fictitious domain stiffness was already applied at the introduction of the finite cell method in [1]. In recent years, the most prominent resolutions to these problems are the application of

*Corresponding author. Tel.: +31 61 516 2599

Email addresses: f.d.prenter@tue.nl (F. de Prenter), c.v.verhoosel@tue.nl (C.V. Verhoosel), e.h.v.brummelen@tue.nl (E.H. van Brummelen)

ghost penalties and element aggregation techniques. The ghost penalty weakly couples the problematic trimmed basis functions to basis functions on neighboring elements through penalties on the jump of (higher-order) derivatives on element boundaries [2, 31] or through volumetric penalization of differences between the solution on a cut element and extrapolations or projections of the solution on neighboring elements [29, 43]. The application of ghost penalties is customary in methods referred to as CutFEM. Aggregation type techniques work in a similar manner, but strongly couple the basis functions on a cut element to basis functions on a particular larger element with a sufficiently large intersection with the physical domain [30, 32, 44–50]. With respect to the conditioning problems in XFEM and GFEM, a notable technique is the Stabilized GFEM (SGFEM) [51, 52], which modifies the enrichment functions such that these are approximately orthogonal to the standard finite element basis functions. This concept of precluding the conditioning problems in XFEM and GFEM through the construction of the enrichment functions is adopted in e.g., [53–55].

In this manuscript, we resolve the ill-conditioning problem of immersed finite element methods by preconditioning of the linear system of equations. This approach has the advantage that it is less intrusive in comparison to the above-mentioned approaches, by virtue of the fact that only the linear algebra aspect of the code is affected. Although the research on preconditioning of immersed isogeometric finite element methods is limited (discussed below), there exists a rich literature on preconditioning for related techniques. Preconditioning techniques for mesh-fitting isogeometric analysis have been studied using a variety of approaches, such as: domain decomposition approaches [56, 57]; Additive-Schwarz preconditioning [58, 59]; multigrid and multilevel preconditioning [60–62] and fast diagonalization [63]. The most notable preconditioning approaches for the conditioning problems of similar origin in XFEM and GFEM are: local Cholesky decompositions [64]; a tailored FETI-type preconditioner [65]; an algebraic multigrid preconditioner based on the Schur complement [66]; and an Additive-Schwarz-type domain decomposition preconditioner [67, 68]. The latter preconditioning technique is conceptually similar to the approach considered in this work. However, direct application of the Additive-Schwarz preconditioner for XFEM to immersed finite elements is impractical, since the number of connected problematic basis functions in immersed finite elements is generally substantially larger than in the XFEM setting. An effective Additive-Schwarz-type preconditioner therefore requires customization to immersed finite element methods.

Dedicated preconditioners have been developed for immersed finite element methods applied to problems resulting in Symmetric Positive Definite (SPD) matrices. In [34] it is demonstrated that a diagonal scaling of trimmed basis functions in combination with an algebraic multigrid preconditioner is effective for linear finite element methods. A Balancing Domain Decomposition by Constraints Preconditioner (BDDC) customized to trimmed basis functions is proposed in [69], which also results in effective preconditioning for linear finite element bases. In [35] we have developed a preconditioner for SPD systems based on a combination of diagonal scaling with local orthonormalization of specific problematic basis functions, and have demonstrated its effectiveness for immersed isogeometric finite element methods.

In this work we explore Additive-Schwarz preconditioning [70–72] for immersed finite element methods. Recent insights into the underlying mechanisms causing ill-conditioning of immersed finite element methods [35] convey that Additive-Schwarz preconditioning is suitable par excellence for resolving these problems. We herein demonstrate that preconditioning based on collections of basis functions supported over trimmed elements, and supplemented with Jacobi preconditioning of the basis functions that are not trimmed, provides an effective general strategy for immersed finite element methods. This tailored Additive-Schwarz preconditioner can also be applied to classes of matrices that are not SPD. Additionally, we demonstrate applicability of the preconditioner to mixed variational forms through preconditioning based on the Schur complement. The preconditioning technique is applicable to higher-order bases with reduced regularity, which enables effective preconditioning of mixed finite element families such as Taylor-Hood [73]. These developments broaden the range of applications and, most notably, open the doors to applications in flow problems. To the best of our knowledge, it is the first preconditioner demonstrated to be effective for immersed (higher-order) finite element discretizations of (Navier-)Stokes systems.

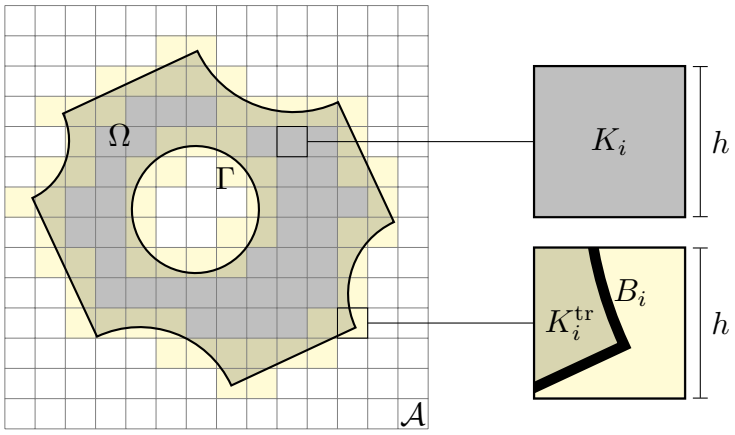

Figure 1: A geometrically complex domain Ω that is encapsulated in a rectilinear ambient domain $\mathcal{A}$. Trimmed elements $K_i^{\mathrm{tr}} \in \mathcal{T}_{\mathcal{C}}^h$ are indicated in yellow, whereas untrimmed elements $K_i \in \mathcal{T}^h \setminus \mathcal{T}_{\mathcal{C}}^h$ are indicated in gray.

The remainder of this manuscript is structured as follows. In Section 2.1 the abstract problem formulation is presented along with a brief review of the conditioning analysis for immersed finite element methods in [35]. The tailored Additive-Schwarz preconditioner is described in Section 3, where we also substantiate the effectiveness of the preconditioner based on the Additive-Schwarz lemma and estimate the computational cost. In Section 4 we demonstrate the effect on both the system condition number and on the solver performance for a range of partial differential equations. Conclusions are drawn in Section 5.

2. Problem formulation and conditioning analysis

2.1. Problem formulation

We consider single-field and mixed partial differential equations posed on a domain $\Omega \subset \mathbb{R}^d$ ($d \in \{2, 3\}$), which we refer to as the physical domain. The boundary $\Gamma = \partial\Omega$ is partitioned in the complementary parts Γ^D and Γ^N for the imposition of Dirichlet and Neumann boundary conditions, respectively. The physical domain is encapsulated by the geometrically simple ambient domain $\mathcal{A}$ on which the tensor product mesh $\mathcal{T}_{\mathcal{A}}^h$ is defined, see Figure 1. We define the mesh of elements intersecting the physical domain as

$$\mathcal{T}^h = \left\{ K_i \in \mathcal{T}_{\mathcal{A}}^h : K_i \cap \Omega \neq \emptyset \right\} \subset \mathcal{T}_{\mathcal{A}}^h, \tag{1}$$

which consists of all elements K_i that intersect the physical domain, and the cut mesh as

$$\mathcal{T}_{\mathcal{C}}^h = \left\{ K_i \in \mathcal{T}^h : K_i \cap \partial\Omega \neq \emptyset \right\} \subset \mathcal{T}^h \subset \mathcal{T}_{\mathcal{A}}^h, \tag{2}$$

which consists of all the trimmed elements. The intersection of an element in $\mathcal{T}_{\mathcal{C}}^h$ with the physical domain is denoted by $K_i^{\mathrm{tr}} = K_i \cap \Omega$ and the intersection of an element with the physical boundary is denoted by $B_i = K_i \cap \Gamma$. In this work we only consider uniform grids, but the presented method is not restricted to this as demonstrated in [74].

On the ambient mesh $\mathcal{T}_{\mathcal{A}}^h$ we define the multivariate isogeometric B-spline basis $\mathcal{N}_{\alpha}^p(\mathcal{T}_{\mathcal{A}}^h)$, which is a tensor product of univariate B-spline bases of degree p and regularity α [4, 75]. Note that, in principle, both p and α can be different per spatial direction and can even vary locally. For simplicity we restrict ourselves to the same global p and α for every spatial direction. The restriction of $\mathcal{N}_{\alpha}^p(\mathcal{T}_{\mathcal{A}}^h)$ to basis functions supported on elements in $\mathcal{T}^h$ is denoted by the basis $\mathcal{N}_{\alpha}^p(\mathcal{T}^h) = \{\phi_i\}_{i=1}^n$. The span of basis $\mathcal{N}_{\alpha}^p(\mathcal{T}^h)$ forms the finite dimensional function space $\mathcal{V}_h(\Omega)$ of dimension n which we employ to approximate the solution to the single-field problems. The solution to two-field mixed problems is approximated in $\mathcal{V}_h(\Omega) \times \mathcal{Q}_h(\Omega)$, which comprises separate

bases for the function spaces $\mathcal{V}_h(\Omega)$ and $\mathcal{Q}_h(\Omega)$. These spaces are generally naturally equipped with inner products, corresponding to the problem under consideration. In the examples in Section 4 we have $\mathcal{V}_h(\Omega) \subset H^1(\Omega)$ and $\mathcal{Q}_h(\Omega) \subset L^2(\Omega)$.

The weak form of the single-field problems we consider herein is written as

$$\begin{cases} \text{Find } u_h \in \mathcal{V}_h(\Omega) \text{ such that:} \\ \qquad a(v_h, u_h) = b(v_h) \quad \forall v_h \in \mathcal{V}_h(\Omega), \end{cases} \tag{3}$$

and that of the two-field mixed problems[1] as

$$\begin{cases} \text{Find } (u_h, p_h) \in \mathcal{V}_h(\Omega) \times \mathcal{Q}_h(\Omega) \text{ such that:} \\ \qquad a_{uu}(v_h, u_h) + a_{up}(v_h, p_h) = b_u(v_h) \quad \forall v_h \in \mathcal{V}_h(\Omega), \\ \qquad a_{up}(u_h, q_h) = b_p(q_h) \quad \forall q_h \in \mathcal{Q}_h(\Omega), \end{cases} \tag{4}$$

where $a(\cdot,\cdot)$ and $b(\cdot)$ are bounded bilinear and linear forms. Note that the Dirichlet boundary conditions are not considered in the construction of the approximation space $\mathcal{V}_h(\Omega)$, but are imposed weakly in the variational form. Different techniques for this exist, of which Nitsche's method [76, 77], the penalty method [78], the nonsymmetric Nitsche method [79–81], and Lagrange multipliers and related methods [82, 83] are the most prevalent. In this contribution we restrict ourselves to the symmetric Nitsche's method and the penalty method. We consider weak problems with higher-order discretizations that are not necessarily Symmetric Positive Definite (SPD) and that are therefore outside the scope of other dedicated preconditioners for immersed finite element methods such as in [34, 35, 69].

In the sequel we will frequently refer to properties of the matrices associated with the weak forms (3) and (4). Using the basis $\mathcal{N}_\alpha^p(\mathcal{T}^h)$ the weak form (3) reduces to the linear system

$$\mathbf{A}\mathbf{x} = \mathbf{b}, \tag{5}$$

where $\mathbf{A}_{ij} = a(\phi_i, \phi_j)$ and $\mathbf{b}_i = b(\phi_i)$ with ϕ_i and ϕ_j denoting the i^{th} and j^{th} basis function, and where $\mathbf{x}$ contains the basis function coefficients in accordance with the discrete solution $u_h = \sum_{i=1}^{n} \phi_i x_i$. Similarly, the mixed form (4) reduces to the linear system

$$\underbrace{\begin{bmatrix} \mathbf{A}_{uu} & \mathbf{A}_{up} \\ \mathbf{A}_{up}^{\mathrm{T}} & \mathbf{0} \end{bmatrix}}_{\mathbf{A}} \underbrace{\begin{pmatrix} \mathbf{x}_u \\ \mathbf{x}_p \end{pmatrix}}_{\mathbf{x}} = \underbrace{\begin{pmatrix} \mathbf{b}_u \\ \boldsymbol{b}_p \end{pmatrix}}_{\mathbf{b}}, \tag{6}$$

where $\mathbf{A}_{uu,ij} = a_{uu}(\phi_i, \phi_j)$, $\mathbf{A}_{up,ik} = a_{up}(\phi_i, \psi_k)$, $\mathbf{b}_{u,i} = b_u(\phi_i)$ and $\mathbf{b}_{p,k} = b_p(\psi_k)$ with ϕ_i and ϕ_j again denoting the i^{th} and j^{th} velocity basis function and ψ_k denoting the k^{th} pressure basis function. The basis function coefficient vectors for the velocity and pressure solutions are denoted by $\mathbf{x}_u$ and $\mathbf{x}_p$, respectively.

2.2. Conditioning of immersed finite element methods

Immersed finite element methods are known to yield severely ill-conditioned systems, see e.g., [7, 8, 34]. In [35] we have shown that these conditioning problems are caused by basis functions that are only supported on small cut elements. Furthermore, it has been established and numerically verified that a scaling relation exists between the condition number and the smallest volume fraction η, which is defined as the smallest relative intersection of an element in $\mathcal{T}^h$ with the physical domain

$$\eta = \min_{K_i \in \mathcal{T}_\mathcal{C}^h} \frac{|K_i \cap \Omega|}{|K_i|} = \min_{K_i \in \mathcal{T}_\mathcal{C}^h} \frac{|K_i^{\text{tr}}|}{|K_i|}. \tag{7}$$

[1] In the remainder we denote the different physical fields by u and p, in reference to the velocity and pressure fields generally considered in mixed flow problems. The presented results are, however, applicable to a general class of mixed problems.

For Symmetric Positive Definite (SPD) matrices derived from immersed formulations of symmetric and elliptic problems, the Euclidean condition number without preconditioning scales with

$$\kappa(\mathbf{A}) = \|\mathbf{A}\|\|\mathbf{A}^{-1}\| = \frac{\lambda_{\max}}{\lambda_{\min}} \propto \eta^{-(2p+1-2/d)}, \tag{8}$$

where $\lambda_{\max}$ and $\lambda_{\min}$ denote the largest and smallest eigenvalue, p denotes the order of the discretization and d denotes the number of spatial dimensions. This relation is derived for SPD matrices, but similar arguments convey that the conditioning of matrices that are not SPD suffer from similar problems. Specifically in three-dimensional problems, volume fractions of $\eta = 10^{-6}$ or smaller are no exception, such that even linear discretizations result in extremely large condition numbers.

The mechanism by which basis functions on small cut elements lead to ill-conditioning can be observed directly from equation (8) (see [35] for details). For an SPD system, the smallest eigenvalue appearing in (8) can be expressed by the Rayleigh quotient

$$\lambda_{\min} = \min_{\mathbf{y}} \frac{\mathbf{y}^T\mathbf{A}\mathbf{y}}{\mathbf{y}^T\mathbf{y}} = \left(\min_{\mathbf{y}} \frac{\|v_h\|}{\|\mathbf{y}\|}\right)^2. \tag{9}$$

The argument of the minimum is the eigenvector corresponding to the smallest eigenvalue, v_h denotes the function corresponding to coefficient vector $\mathbf{y}$ and $\|v_h\|^2 = a(v_h, v_h)$ denotes the energy norm induced by the weak formulation. The eigenvalue $\lambda_{\min}$, hence, becomes very small when the function norm becomes very small compared to the norm of the coefficient vector, i.e., $\|v_h\| \ll \|\mathbf{y}\|$. In [35] it is shown that this critical mode, v_h, is related to trimmed basis functions that are only supported on the cut element with the smallest volume fraction. These basis functions cause ill-condition in two ways: *i)* a single trimmed basis function can have a small norm because its support over the physical domain is very small; *ii)* trimmed basis functions can become almost linearly dependent on small cut elements, which implies that a vector $\mathbf{y}$ can be constructed such that $\|v_h\| \ll \|\mathbf{y}\|$. Such almost linear dependencies between trimmed basis functions can occur for linear bases and higher-order bases with maximum regularity for specifically-shaped trimmed elements. For higher-order bases with reduced regularity, almost linear dependencies generally occur on elements with small volume fractions of arbitrary shape.

Ill-conditioning caused by basis functions with a small norm can be effectively remedied by diagonal scaling or Jacobi preconditioning, which scales the basis functions such that these all have the same norm. Almost linear dependencies of trimmed basis functions are not resolved by diagonal scaling, and require a preconditioning strategy that accounts for the interdependence of basis functions. The ineffectiveness of Jacobi preconditioning for ill-conditioning caused by almost linear dependencies is for example observed in the results for quadratic Lagrange bases in [35, Figure 6]. In the remainder of this manuscript a preconditioner is proposed that effectively remedies both above-mentioned causes of ill-conditioning.

Remark 2.1. *Since the conditioning problems of immersed finite element methods originate from small eigenvalues caused by cut elements with small volume fractions, the quotient between the absolute largest and smallest eigenvalue is a good indicator of the cut element conditioning problem*[2]*. To demonstrate the robustness of the preconditioner to cut elements in Section 4, we therefore do not only consider the convergence of iterative solvers but also report this quotient. The observed correspondence between the condition numbers and the iterative-solver convergence stipulates that the ill-conditioning caused by small cut elements indeed determines solver performance, which is in agreement with theoretical results, see e.g., [84].*

[2]For symmetric matrices the quotient between the absolute largest and smallest eigenvalue is equal to the condition number and for nonsymmetric matrices this quotient bounds the condition number from below.

3. Tailored Additive-Schwarz preconditioning for immersed finite element methods

In this section we propose a tailored Additive-Schwarz preconditioner for the immersed finite element setting introduced in Section 2.1. In Section 3.1 we discuss the formal definition of Additive-Schwarz preconditioners [70–72], along with the specific selection of the index blocks. In Section 3.2 we analyze the effectiveness of this selection for the specific conditioning problems of immersed finite element methods. In Section 3.3 we finally discuss the computational complexity of the iterative solution procedure.

3.1. Additive-Schwarz block selection

Additive-Schwarz preconditioning of a matrix $\mathbf{A} \in \mathbb{R}^{n \times n}$ relies on the selection of a set of $N \geq 1$ blocks of indices (subsets) corresponding to basis functions. We denote the index blocks as $\{\mathcal{K}_i\}_{i=1}^{N}$ and the cardinality of each block as $m_i = \#\mathcal{K}_i$. Given the index blocks, a preconditioner for the matrix $\mathbf{A}$ is constructed as

$$\mathbf{S} = \sum_{i=1}^{N} \mathbf{P}_i \underbrace{\left(\mathbf{P}_i^T \mathbf{A} \mathbf{P}_i\right)^{-1}}_{\mathbf{A}_i^{-1}} \mathbf{P}_i^T, \tag{10}$$

where the prolongation operator $\mathbf{P}_i \in \mathbb{R}^{n \times m_i}$ consists of the unit vectors corresponding to the indices in block $\mathcal{K}_i$, i.e., $\mathbf{P}_i = [\mathbf{e}_{\mathcal{K}_i(1)}, ..., \mathbf{e}_{\mathcal{K}_i(m_i)}]$, and where the restriction operator $\mathbf{P}_i^T$ is defined as the transpose of the prolongation operator. If the index blocks are sufficiently small, the block matrices $\mathbf{A}_i = \mathbf{P}_i^T \mathbf{A} \mathbf{P}_i$ can be inverted to form $\mathbf{A}_i^{-1}$. It is implicitly assumed that the block matrices are invertible, which is the case for all our examples in Section 4 as these derive from coercive bilinear forms. Each of the inverted block matrices $\mathbf{A}_i^{-1}$ is transferred to an $n \times n$ matrix using the prolongation and restriction matrices, i.e., $\mathbf{P}_i \mathbf{A}_i^{-1} \mathbf{P}_i^T$, resulting in a sparse matrix with only m_i^2 nonzero entries at the cross indices of block $\mathcal{K}_i$. These sparse matrices are summed to form the Additive-Schwarz preconditioner $\mathbf{S}$ in accordance with equation (10).

An Additive-Schwarz preconditioner that is tailored to the conditioning problems of scalar, single-field immersed finite element methods can be constructed by exploiting geometrical knowledge about the connectivity of basis functions based on intersecting supports on an element. For element K_i the index block $\mathcal{K}_i$ is devised, consisting of the indices of the basis functions supported on element K_i. Since the ill-conditioning problem of immersed finite element methods originates from the cut elements, for reasons of efficiency we only device blocks for the cut elements in $\mathcal{T}_{\mathcal{C}}^h$. This leaves out untrimmed basis functions, i.e., basis functions that are not supported on any of the cut elements. These basis functions are not prone to almost linear dependencies, however, such that for these basis functions a simple diagonal scaling suffices. This can be conceived of as devising a separate 1×1 block for each basis function that is not trimmed.

This procedure for single-field problems can be applied directly to vector-valued problems such as linear elasticity. However, the structure of such problems can be leveraged to reduce the computational effort involved in the construction of the preconditioner. Since basis functions for different geometrical directions are inherently linearly independent (see Remark 3.2), these cannot become almost linearly dependent by the mechanism described in Section 2.2. Hence, the interdependence of such basis functions does not need to be taken into consideration in the construction of the preconditioner. This implies that it is possible to select separate index blocks for different geometrical directions. A preconditioner can then be constructed by direct application of the single-field Additive-Schwarz preconditioner proposed above to each of the geometrical directions.

For mixed problems such as (Navier-)Stokes the basis functions describing the different physical fields can also not become almost linearly dependent. In general, basis functions of different physical fields can therefore be treated separately to reduce the computational effort involved in the construction of the preconditioner. However, direct application of (10) to $\mathbf{A}_{pp}$ is often impossible, as for most formulations this pressure block cannot be inverted. To circumvent this problem, we therefore construct the above described tailored Additive-Schwarz preconditioner for

the pressure field based on an approximation of the Schur complement $\mathbf{A}_{up}\mathbf{A}_{uu}^{-1}\mathbf{A}_{up}^T$, see e.g., [85]. As pressure functions in (Navier-)Stokes are applied as L^2-functions, approximating the Schur complement by the mass (or L^2-projection) matrix is sufficient to scale and resolve the almost linear dependencies in the pressure space. Let us note, however, that different approaches can be adopted for preconditioning immersed mixed problems, based on alternative approximations of the Schur complement, see e.g., [86]. We have also considered approximations of the Schur complement of the form $\mathbf{A}_{up}\mathbf{S}(\mathbf{A}_{uu})\mathbf{A}_{up}^T$, with $\mathbf{S}(\mathbf{A}_{uu})$ the Additive-Schwarz preconditioner of $\mathbf{A}_{uu}$. Another option pertains to the use of preconditioners based on Vanka-type smoothers [87]. We have obtained similar results with these alternative preconditioning strategies. In Section 4 we restrict our investigation of mixed problems to the tailored Additive-Schwarz preconditioner for the pressure field based on the mass matrix as approximate Schur complement.

Remark 3.1. *While the Additive-Schwarz preconditioner discussed above is conceptually different from the SIPIC preconditioner in [35], these preconditioners are related. In both preconditioners, blocks are selected which contain basis functions that can become almost linearly dependent. The tailored Additive-Schwarz preconditioner described herein selects overlapping blocks by exploiting geometrical knowledge, whereas the SIPIC algorithm algebraically selects disjoint blocks of indices that can become almost linearly dependent to each other. The symmetrically applied SIPIC preconditioner then orthonormalizes the basis functions in a block by a Gram-Schmidt procedure. When applied as a left preconditioner, SIPIC becomes a block Jacobi matrix, which is basically an Additive-Schwarz preconditioner with disjoint blocks. The tailored Additive-Schwarz preconditioner developed herein differs in the way the Additive-Schwarz blocks are selected. We have found that the overlapping blocks based on geometrical knowledge are more robust and more efficient for high-order bases with reduced regularity, such as Lagrange bases and Taylor-Hood bases [73]. This is because for such bases the algebraic selection of disjoint blocks as in SIPIC does not necessarily detect all the potential almost linear dependencies. Moreover, it can also result in very large blocks, leading to a large computational cost. The geometrical selection of overlapping blocks as used in the Additive-Schwarz preconditioner in this work does not suffer from this.*

3.2. Effectiveness of the preconditioner

Equation (10) conveys that the preconditioner $\mathbf{S}$ is a summation of block-wise inverses of $\mathbf{A}$, from which it is natural to interpret $\mathbf{S}$ as a sparse approximation of $\mathbf{A}^{-1}$. We consider the Additive-Schwarz lemma to describe why the preconditioner $\mathbf{S}$ using the block selection as discussed in Section 3.1 effectively resolves the specific cut-element related ill-conditioning discussed in Section 2.2. This lemma states that for a Symmetric Positive Definite (SPD) matrix $\mathbf{A}$, the following holds [88, 89] (see [70, 71] for this specific form)

$$\mathbf{y}^T\mathbf{S}^{-1}\mathbf{y} = \min_{\mathbf{y}=\sum_{j=1}^{N}\mathbf{P}_j\tilde{\mathbf{y}}_j} \sum_{i=1}^{N} \tilde{\mathbf{y}}_i^T\mathbf{A}_i\tilde{\mathbf{y}}_i = \min_{\mathbf{y}=\sum_{j=1}^{N}\mathbf{P}_j\tilde{\mathbf{y}}_j} \sum_{i=1}^{N} \left(\mathbf{P}_i\tilde{\mathbf{y}}_i\right)^T\mathbf{A}\left(\mathbf{P}_i\tilde{\mathbf{y}}_i\right) \quad \forall \mathbf{y}\in\mathbb{R}^n. \tag{11}$$

This equation conveys that the $\mathbf{S}^{-1}$-inner product of an arbitrary vector $\mathbf{y}\in\mathbb{R}^n$ is equal to the minimum of the sum of the $\mathbf{A}_i$-inner products of the block vectors $\tilde{\mathbf{y}}_i\in\mathbb{R}^{m_i}$ over all sets of block vectors that sum to $\mathbf{y}$. A set of block vectors whose prolongations accumulate into $\mathbf{y}$ exists for all vectors $\mathbf{y}\in\mathbb{R}^n$ if and only if every index is in at least one of the index blocks $\mathcal{K}_i$. When the blocks overlap, which is the case here since basis functions are generally supported on more than one cut element, multiple sets of block vectors that sum to $\mathbf{y}$ exist.

To relate equation (11) to the cut-element related ill-conditioning problem, we consider a function v_h that is a linear combination of almost linearly dependent basis functions. Section 2.2 conveys that the coefficient vector $\mathbf{y}$ corresponding to v_h can yield a very small Rayleigh quotient with matrix $\mathbf{A}$. For the basis functions that construct v_h to be almost linearly dependent, these basis functions must intersect on a small cut element. Hence, these basis functions are by construction together in one index block, $\mathcal{K}_i$. Consequently, the coefficient vector $\mathbf{y}$ corresponding to v_h can be written as the prolongation of a single block vector, i.e., $\mathbf{y}=\mathbf{P}_i\tilde{\mathbf{y}}_i$. From equation (11) it

follows that the Rayleigh quotient of $\mathbf{y}$ with $\mathbf{S}^{-1}$ is bounded from above by the Rayleigh quotient with $\mathbf{A}$, and hence is also very small. From this it is concluded that $\mathbf{S}^{-1}$ captures the problematically small eigenmodes that are specific to matrices derived from immersed finite element methods, which makes $\mathbf{S}$ an effective preconditioner to resolve these problems.

We note that the shape of the boundary or the geometry of a cut element is not considered in the preconditioning scheme. In Section 2.2 it is mentioned that certain cut elements contain certain basis functions that are prone to almost linear dependencies, while for many cut basis functions Jacobi preconditioning suffices. This can be observed in the numerical results in Section 4, which show that the performance of a Jacobi preconditioner is non-robust and highly dependent on the test case. The implementation of an algorithm to determine from the geometry whether basis functions are prone to almost linear dependencies is, however, invasive and requires geometrical information that is not generally accessible in numerical codes. Therefore a block is assigned to every element in $\mathcal{T}_{\mathcal{C}}^{h}$ as described in Section 3.1.

The proposed preconditioner does not depend on the applied boundary conditions. Since the specific conditioning problems of immersed finite element methods originate from basis functions that become almost linearly dependent, the type of boundary condition in general plays a minor role. This is confirmed by the results of the numerical simulations in Section 4. An exception to this is the case in which boundary conditions lead to a coupling of basis functions in different spatial directions, see Remark 3.2. Such exceptional cases can also be preconditioned effectively by gathering the problematic basis functions in different spatial dimensions in one index block.

Equation (11) is in principle restricted to SPD matrices, but Additive-Schwarz preconditioners, for which equation (10) forms the basis, have been investigated extensively for nonsymmetric and indefinite systems [70, 71, 90–97] and have successfully been applied to mesh-conforming Navier-Stokes systems, see e.g., [98]. In Section 4 we present results for both SPD and non-SPD matrices. The considered non-SPD matrices still derive from coercive formulations, as is the case for many partial differential equations such as problems involving convection and bilinear forms resulting from the nonsymmetric Nitsche formulation, see e.g., [79, 81, 99]. The non-SPD matrices in Section 4 can therefore be considered as sums of both SPD and non-SPD contributions, with the relative strength of the SPD character of the resulting matrices depending on factors as the mesh-size, the Péclet or Reynolds number and potentially Streamline Upwind/Petrov-Galerkin (SUPG) or Variational MultiScale (VMS) stabilization terms [100–103]. We have observed the Additive-Schwarz preconditioner to be effective for all the examples presented in Section 4, but a dedicated study for the effect of the relative strength of the SPD-character of the matrix is considered beyond the scope of the current work.

Remark 3.2. *While the proposed preconditioner is robust with respect to the most commonly applied boundary conditions, modifications to the block selections can be required in the case that boundary conditions introduce almost linear dependencies between basis functions in different spatial directions. Examples of such boundary conditions are non-penetration boundary conditions, prescribed normal displacements or boundary conditions on nearly incompressible materials. The reason that these boundary conditions can introduce almost linear dependencies is that the bilinear forms related to such boundary conditions associate a much larger penalty or energy to velocities or displacements normal to the boundary than to velocities or displacements tangential to the boundary. Basis functions describe a velocity or displacement in an elementary geometrical direction that is generally not aligned with or perpendicular to the normal of the boundary. Therefore, basis functions in different elementary geometrical directions both contain a high-energy normal component and a low-energy tangential component. With very large Nitsche penalties on small cut elements, the tangential component is completely dominated by the normal component. These basis functions in different elementary geometrical directions can then become almost linearly dependent to each other, which directly violates the selection procedure in Section 3.1. This can be resolved by adding the functions in different geometrical directions to the same Additive-Schwarz block, but for conciseness this is not presented in the results in Section 4.*

Remark 3.3. *Since small cut elements yield correspondingly small eigenvalues, it is possible that the system contains eigenvalues that are, in absolute sense, smaller than machine precision. When this occurs, round-off errors can play a significant role, such that inverses of the block matrices can be inaccurate. This generally impedes the convergence of a Conjugate Gradient solver as observed in [74]. In GMRES, round-off errors can cause failures in the orthogonalization of the vectors that span the Krylov space (see Section 4, Figure 21). Since these problematic eigenmodes with eigenvalues below machine precision do not significantly affect the accuracy of the solution, we dispose of these eigenmodes by removing specific basis functions using Algorithm 1. For the single-field problems and the velocity matrices in (Navier-)Stokes in Section 4 a relative threshold of* 10^{-14} *was found to yield stable results. The preconditioner of the pressure space required a stricter threshold, which we attribute to discrepancies between the round-off errors in the system matrix and the pressure mass matrix by which the Schur complement is approximated. Therefore the threshold for the pressure space was set three orders of magnitude larger than the threshold for the velocity space to* 10^{-11}*. This is still approximately two orders of magnitude smaller than the tolerance of the GMRES solver that was set to* $2^{-30} \approx 10^{-9}$*, such that this does not significantly affect the accuracy of the solution. Note that this procedure is conceptually similar to the basis function removal in [104], but differs in the threshold value and in the fact that Algorithm 1 still removes a basis function when basis functions that are all larger than the threshold can form a linear combination that is smaller than the threshold. For this reason Algorithm 1 is also applicable to bases with reduced continuity.*

Algorithm 1: eliminate($\mathbf{A}$, $\{\mathcal{K}_i\}_{i=1}^N$, *relativeThreshold*)

```
# initialize
referenceValue = relativeThreshold*max(diagonal(A))  # absolute reference
eliminatedFuncs = set()  # empty set of eliminated functions

# loop over blocks
for K_j ∈ {K_i}_{i=1}^N do
    stable = False  # block initially assumed unstable
    # eliminate functions until block is stable
    while not stable do
        A_j = A_{K_j,K_j}  # block-matrix
        eigVals, eigVecs = eig(A_j)  # eigenvalues
        smallestValue = min(abs(eigVals))  # smallest absolute eigenvalue
        if smallestValue < referenceValue then
            # block-matrix unstable: eliminate most unstable basis function
            smallestMode = argMin(abs(eigVals))  # local index smallest eigenvalue
            eigVec = eigVecs(smallestMode)  # block-eigenvector
            localFunc = argMax(abs(eigVec))  # local index dominant basis function
            globalFunc = K_j(localFunc)  # global index
            eliminatedFuncs.append(globalFunc)  # add to eliminated functions
            K_j.delete(globalFunc)  # remove from block
        else
            # block-matrix stable: exit while-loop
            stable = True
        end
    end
end

return eliminatedFuncs
```

3.3. Computational cost

The computational cost of setting up the Additive-Schwarz preconditioner consists of two components, *viz.* the floating point operations involved in inverting the block matrices and the memory required for storing the preconditioner. The number of block matrices depends on the number of cut elements and the number of solution variables. The number of block matrices can therefore vary from negligible, in case most elements are not cut, to linear with the number of degrees of freedom (DOFs), in case the majority of the elements is cut. The block matrices have a small size of $(p+1)^d$, with p the order of the discretization and d the number of dimensions. Consequently, computing these inverses is inexpensive and, in our experience, negligible compared to the computational cost of quadrature on the cut elements. Furthermore, this operation is highly parallelizable. The memory required to store the preconditioner is also approximately linear with the number of cut elements, and can vary from negligible to linear with the number of DOFs. In case all elements are cut, the preconditioner of a solution variable contains a nonzero entry at a cross index when the two corresponding basis functions intersect. This implies that the preconditioner of a solution variable has the same sparsity structure as the system matrix. Since the preconditioner does not contain cross terms between separate solution variables (d nonzero blocks instead of d^2 for the system matrix), the memory required to precondition a vector problem such as linear elasticity is approximately $\frac{1}{d}$ of the memory required to store the system matrix, in case all elements are cut.

A preconditioned Conjugate Gradient solver multiplies a vector with both the system matrix and the preconditioner at every iteration. Because the number of nonzero entries in the preconditioner is smaller than the number of nonzero entries in the system matrix, the cost of these two multiplications is linear with the number of DOFs, i.e., $\mathcal{O}(n)$. From the results in Section 4 it follows that the required number of iterations is inversely proportional to the mesh size, i.e., $\mathcal{O}(h^{-1}) = \mathcal{O}(n^{\frac{1}{d}})$, which is in correspondence with the literature, e.g., [84]. The total computational cost of solving the linear system with a Conjugate Gradient solver is therefore of order $\mathcal{O}(n) \cdot \mathcal{O}(n^{\frac{1}{d}}) = \mathcal{O}(n^{1+\frac{1}{d}})$ (or, equivalently, $\mathcal{O}(h^{-(d+1)})$). The observed CPU times for solving the linear systems of the three-dimensional elasticity problem in Section 4 verify this scaling relation.

The computational cost of the GMRES solver that is applied for the non-SPD matrices scales slightly differently with the number of DOFs. The convergence analysis of GMRES is less straightforward, see e.g., [84], but also for GMRES we observe in Section 4 that the required number of iterations is approximately inversely proportional to the mesh size, i.e., $\mathcal{O}(n^{\frac{1}{d}})$. For GMRES the cost of an iteration also scales with the number of DOFs, however, the total cost of GMRES is approximately quadratic with the number of iterations through the orthonormalization of the vectors that span the Krylov space, i.e., $\mathcal{O}(n^{\frac{2}{d}})$. The total cost of solving a system by GMRES therefore is of order $\mathcal{O}(n^{1+\frac{2}{d}})$ (or, equivalently, $\mathcal{O}(h^{-(d+2)})$). This scaling relation is verified by consideration of the CPU time for solving the linear systems of the three-dimensional Stokes problem in Section 4. Because GMRES explicitly stores the Krylov space, its memory requirements must be taken into consideration. With the observed numbers of iterations, the required memory scales with the number of DOFs as $\mathcal{O}(n^{1+\frac{1}{d}})$. Note that, although not considered in this work, restarted GMRES can potentially reduce the scaling rates of both the computation time and memory.

Considering the resemblance with mesh-fitting methods in terms of the number of iterations, we anticipate that the required number of iterations can potentially be made independent of the number of DOFs by incorporation of the developed preconditioner in a multigrid framework, e.g., [84, 105, 106]. This would bring down the total cost of both solvers to $\mathcal{O}(n)$.

4. Numerical examples

In this section we study the effectiveness and performance of the tailored Additive-Schwarz preconditioner based on several representative two- and three-dimensional numerical test cases. To assess the versatility of the Additive-Schwarz preconditioner in the context of immersed finite element methods we compare it to a standard Jacobi preconditioner. This comparison specifically demonstrates the conditioning effect of immersed discretizations, because these preconditioners are

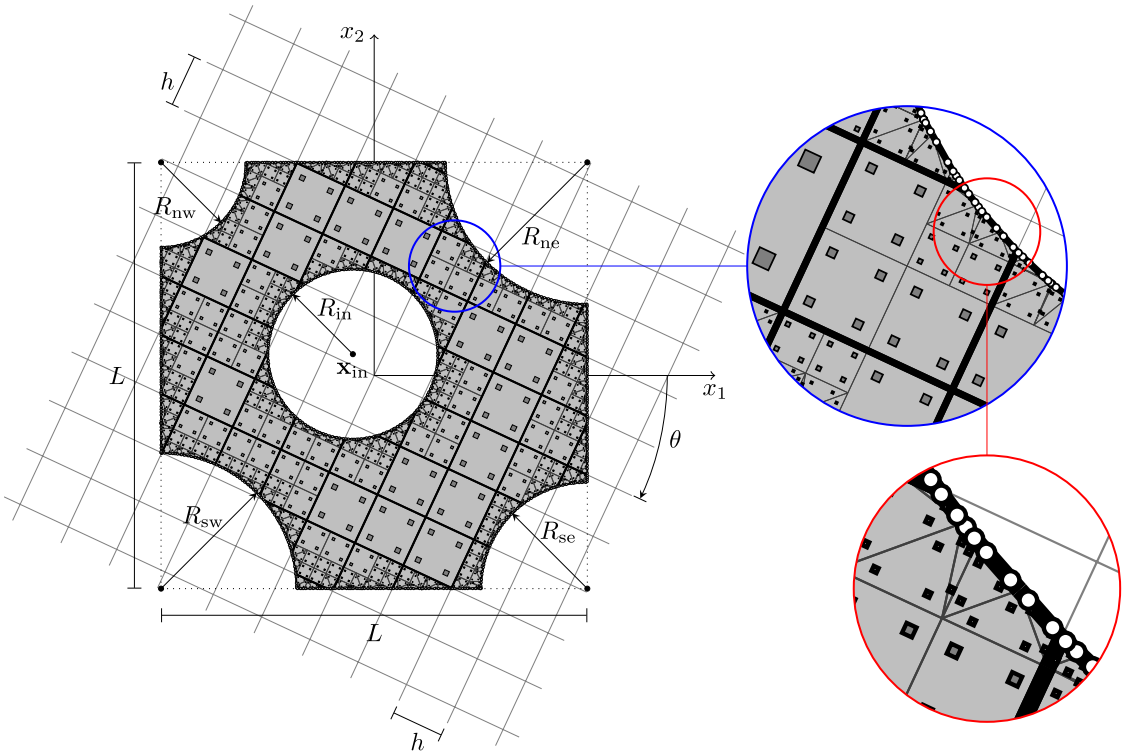

Figure 2: Schematic representation of the physical domain immersed in a background grid, which is rotated with respect to the physical domain over an angle θ. Numerical integration is performed using the integration procedure outlined in [107]. In this integration procedure elements intersecting the boundary of the physical domain are recursively bisectioned, until a maximum bisectioning depth is achieved. At this lowest level a triangulation algorithm is applied. For each of the integration subcells standard Gauss quadrature rules are employed for the evaluation of interior integrals (gray squares). The edges of the lowest level integration subcells that approximate the boundary of the physical domain are used to construct the quadrature points for the evaluation of boundary integrals (white circles).

the same on untrimmed elements and only differ in the treatment of cut elements. In Section 4.1 we consider an elasticity problem, which results in a SPD system that is solved using a Conjugate Gradient solver. An SUPG-stabilized convection-dominated convection-diffusion problem with a nonsymmetric but coercive weak form is then considered in Section 4.2, where use is made of a GMRES solver. Section 4.3 is concerned with a Stokes flow problem, which results in a symmetric indefinite mixed system, which is preconditioned using the approximate Schur complement and solved using GMRES. Finally, in Section 4.4 a Navier-Stokes flow problem yielding a nonsymmetric and indefinite mixed matrix is studied. Also this problem is preconditioned using the approximate Schur complement and solved using GMRES.

All two-dimensional problems are posed on the domain illustrated in Figure 2. Numerical integration is based on the procedure introduced in [107] with an integration depth of 3, which is illustrated schematically in Figure 2. The size of the square bounding box of the physical domain is $L = 1$. The radii of the circular corner exclusions are taken as $R_{\text{ne}} = \frac{1}{3}$, $R_{\text{nw}} = \frac{1}{5}$, $R_{\text{sw}} = \frac{1}{\pi}$, and $R_{\text{se}} = \frac{1}{4}$. The radius of the interior circular exclusion positioned at $\mathbf{x}_{\text{in}} = (-\frac{1}{20}, \frac{1}{20})$ is given by $R_{\text{in}} = \frac{1}{5}$. We rotate the grid over a total angle of $\theta = 45^\circ$ in 20 steps. The stepwise rotations of the grid yield different discretizations with different cut elements of the same problem with the same mesh size. This enables an investigation of the robustness of both the tailored Additive-Schwarz and the diagonal Jacobi preconditioner. The advantage of the two-dimensional problems is that the largest and smallest eigenvalues and the iterative solutions of all the systems can be computed at an acceptable computational cost. Following the analysis and results in [35, page 316], the specific conditioning problems of immersed finite element methods are not affected by the size

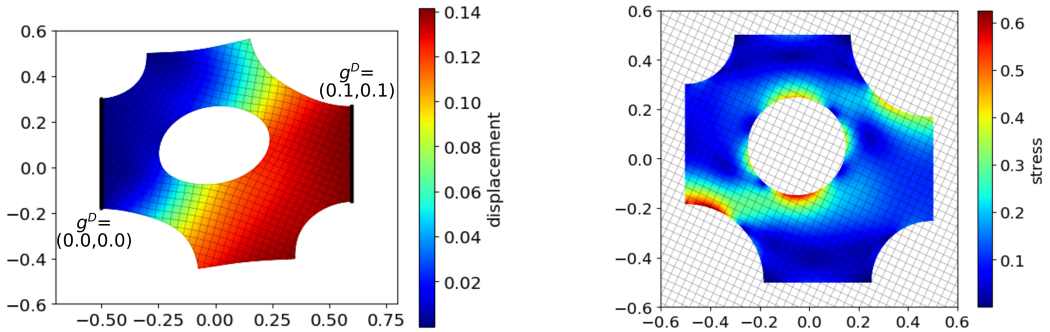

(a) Displacement magnitude

(b) Frobenius norm of stress tensor

Figure 3: Boundary conditions and solution of the 2D elasticity problem in (12). The Dirichlet boundary Γ^D is indicated by the thick black lines in (a). Figure (a) shows the deformed and (b) the undeformed geometry. Note that the deformed mesh is only plotted inside the physical domain since there is no solution for the deformation in the fictitious domain.

of the problem, which makes this investigation representative for more complex problems. The applicability of the preconditioner to computationally challenging three-dimensional problems is demonstrated for an elasticity problem on a trabecular bone specimen and for Stokes and Navier-Stokes flow problems around an object with the shape of a popcorn flake.

Detailed numerical investigations into the effect of the grid size and the discretization order are performed by considering grid sizes of $h = \frac{1}{16}$, $h = \frac{1}{32}$, and $h = \frac{1}{64}$ and discretization orders of $p = 1$, $p = 2$, and $p = 3$. The presented test cases cover aspects such as the effect of different boundary conditions, the shape of the boundary, or the geometry of the cut elements, but isolated investigations into these effects will not be presented.

4.1. Linear elasticity problems

We consider the linear elasticity problem ignoring inertia effects and body forces

$$\begin{cases} \operatorname{div}(\boldsymbol{\sigma}) = \mathbf{0} & \text{in } \Omega, \\ \boldsymbol{u} = \boldsymbol{g}^D & \text{on } \Gamma^D, \\ \boldsymbol{\sigma}\boldsymbol{n} = \boldsymbol{g}^N = \mathbf{0} & \text{on } \Gamma^N, \end{cases} \tag{12}$$

with Cauchy stress tensor $\boldsymbol{\sigma} = \boldsymbol{\sigma}(\boldsymbol{u}) = \lambda \operatorname{div}(\boldsymbol{u})\mathbf{I} + 2\mu\nabla^s\boldsymbol{u}$, dimensionless Lamé parameters $\lambda = \mu = 1$, and ∇^s denoting the symmetric gradient operator. Figure 3 shows the partitioning of the boundary into Γ^D and Γ^N, the boundary conditions, and the solution with a grid of $h = \frac{1}{32}$ at an angle of 22.5° using quadratic B-splines.

The variational form of the problem with boundary conditions imposed by Nitsche's method [76] is

$$\begin{cases} \text{Find } \boldsymbol{u}_h \in \mathcal{V}_h(\Omega) \text{ such that for all } \boldsymbol{v}_h \in \mathcal{V}_h(\Omega): \\ \\ \int_\Omega \nabla^s\boldsymbol{v}_h : \boldsymbol{\sigma}(\boldsymbol{u}_h)\,\mathrm{d}V + \int_{\Gamma^D} -\boldsymbol{v}_h \cdot \boldsymbol{\sigma}(\boldsymbol{u}_h)\boldsymbol{n} - \boldsymbol{u}_h \cdot \boldsymbol{\sigma}(\boldsymbol{v}_h)\boldsymbol{n}\,\mathrm{d}S \\ \qquad + \int_{\Gamma^D} \lambda\beta^\lambda(\boldsymbol{v}_h \cdot \boldsymbol{n})(\boldsymbol{u}_h \cdot \boldsymbol{n}) + 2\mu\beta^\mu\boldsymbol{v}_h \cdot \boldsymbol{u}_h\,\mathrm{d}S \\ \\ = \int_{\Gamma^D} -\boldsymbol{g}^D \cdot \boldsymbol{\sigma}(\boldsymbol{v}_h)\boldsymbol{n}\,\mathrm{d}S + \int_{\Gamma^D} \lambda\beta^\lambda(\boldsymbol{v}_h \cdot \boldsymbol{n})(\boldsymbol{g}^D \cdot \boldsymbol{n}) + 2\mu\beta^\mu\boldsymbol{v}_h \cdot \boldsymbol{g}^D\,\mathrm{d}S. \end{cases} \tag{13}$$

This formulation with separate penalization for the Lamé parameters was proposed in [8] and yields an SPD matrix. The separate element-wise stabilization constants are defined as[3]

$$\beta^{\lambda}\big|_{K_i} = 2 \max_{\boldsymbol{v}_h \in \mathcal{V}_h(\Omega)} \frac{\|\mathrm{div}(\boldsymbol{v}_h)\|^2_{L^2(B_i^D)}}{\|\mathrm{div}(\boldsymbol{v}_h)\|^2_{L^2(K_i^{\mathrm{tr}})}}, \tag{14}$$

and

$$\beta^{\mu}\big|_{K_i} = 2 \max_{\boldsymbol{v}_h \in \mathcal{V}_h(\Omega)} \frac{\|\left(\nabla^s \boldsymbol{v}_h\right)\boldsymbol{n}\|^2_{L^2(B_i^D)}}{\|\nabla^s \boldsymbol{v}_h\|^2_{L^2(K_i^{\mathrm{tr}})}}, \tag{15}$$

and can be computed by solving a local generalized eigenvalue problem following the approach in [77]. To improve the conditioning of this generalized eigenvalue problem we perform a local change of basis, as described in [35, Appendix A]. For shape-regular trimmed elements it holds that $\beta^{\lambda,\mu}_{K_i} \sim |B_i^D|/|K_i^{\mathrm{tr}}| \sim 1/\hat{h}_{K_i}$ with $\hat{h}_{K_i}$ the typical length scale of the trimmed element K_i^{tr} [108].

Figure 4 displays the condition number[4] and the CG convergence in terms of the residual and error for the Additive-Schwarz-preconditioned, Jacobi-preconditioned and unpreconditioned systems for $h = \frac{1}{32}$ and quadratic B-splines. The systems comprise approximately 1 850 degrees of freedom. Figure 4a shows that the systems without any preconditioning are severely ill-conditioned. The diagonally scaled matrices are conditioned significantly better than the unpreconditioned systems. For certain rotation angles the systems with Jacobi preconditioning are well-conditioned, while for other angles the eigenvalue ratios are still large. This effect is explained in Section 2.2, since on cut elements of certain geometries Jacobi preconditioning suffices as these are not prone to almost linear dependencies, while on other cut elements the almost linear dependencies render Jacobi preconditioning inadequate. This non-robust behavior is typical for small systems, as for large systems it is unlikely that none of the cut elements is prone to almost linear dependencies. Figures 4b and 4c show the convergence of a Conjugate Gradient solver that is terminated when either the residual is reduced by $2^{-30} \approx 10^{-9}$ or when the number of iterations reaches 10^4. Figure 4b shows the convergence of the relative residual, $\|\mathbf{b} - \mathbf{A}\mathbf{x}_i\|/\|\mathbf{b}\|$, and Figure 4c presents the convergence of the relative error in the energy norm, $\left((\mathbf{x} - \mathbf{x}_i)^T\mathbf{A}(\mathbf{x} - \mathbf{x}_i)/\mathbf{x}^T\mathbf{A}\mathbf{x}\right)^{1/2}$, with $\mathbf{x}$ the solution obtained with a direct solver. It is visible that the systems without preconditioning hardly converge. The convergence of the Jacobi preconditioned systems is erratic, similar to the eigenvalue ratios. It is important to note that for all these systems the residual is ultimately reduced by 2^{-30}, while for certain rotations the reduction of the error in the energy norm is much less. The systems that are preconditioned by the Additive-Schwarz preconditioner all converge in approximately 200 iterations and converge robustly in both the residual and the energy norm.

The effect of the grid size on the performance of the Additive-Schwarz preconditioner is investigated by comparing results for quadratic B-spline bases with grid sizes of $h = \frac{1}{16}$, $h = \frac{1}{32}$, and $h = \frac{1}{64}$ in Figure 5. The systems contain approximately 600, 1 850 and 6 300 degrees of freedom for the different grid sizes. Figure 5a demonstrates that the eigenvalue ratios are virtually independent of the cut elements and are approximately proportional to h^{-2}. This h-dependence is consistent with the literature for mesh-fitting discretizations, see e.g., [109, 110]. The consistent convergence of the Conjugate Gradient solver for the different rotations in Figures 5b and 5c shows that for all grid sizes the preconditioner is robust. The number of iterations is approximately inversely proportional to the mesh size, which is also in accordance with the literature for mesh-fitting discretizations, see e.g., [84].

In Figure 6 we investigate the effect of the discretization order by comparing linear, quadratic and cubic B-splines with optimal regularity on a grid with $h = \frac{1}{32}$. The systems with the different discretization orders have a size of approximately 1 650, 1 850 and 2 050 degrees of freedom. One

[3] See Figure 1 for the definition of K_i, K_i^{tr}, and B_i^D.

[4] Using a power algorithm, the condition number can be computed at an acceptable computational cost for all two-dimensional systems considered in this section.

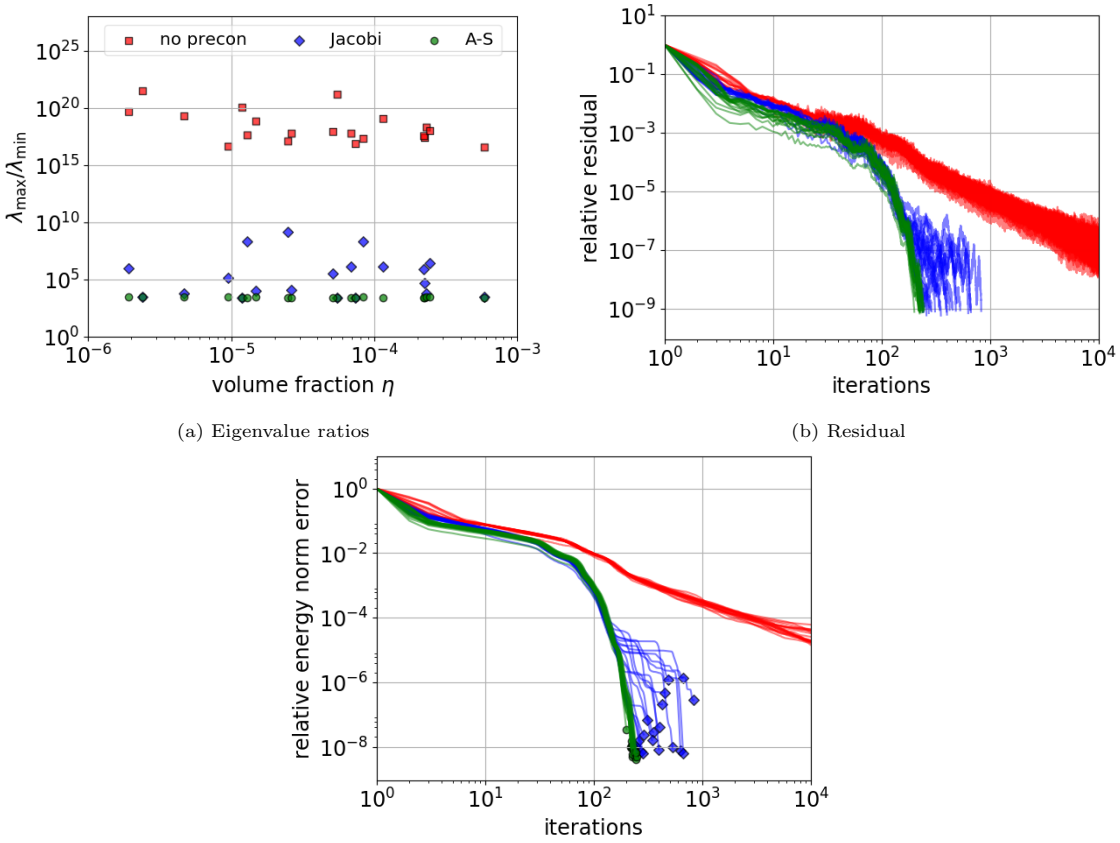

(a) Eigenvalue ratios

(b) Residual

(c) Error in the energy norm

Figure 4: Comparison of the Additive-Schwarz preconditioned, Jacobi preconditioned and unpreconditioned system with grids of $h = \frac{1}{32}$ using quadratic B-spline bases for the 2D elasticity problem for all rotation angles.

can observe that the eigenvalue ratios and the convergence are not affected by the rotations for different discretization orders and that the iteration counts correspond to the eigenvalue ratios, see e.g., [84]. It is remarkable that the eigenvalue ratios and the convergence are slightly better for higher orders, which is not consistent with the literature on mesh-fitting isogeometric discretizations, see e.g., [110]. The observed dependence on the discretization order is small, however, and the investigated orders are lower than in [110]. Furthermore, it should be noted that for higher orders the Additive-Schwarz blocks are larger because more basis functions are supported on an element, which possibly affects the eigenfunctions. In conclusion, we observe that the tailored Additive-Schwarz preconditioner is robust for different discretization orders.

To demonstrate the effectiveness of the preconditioner on a three-dimensional problem, we consider the μCT-scan of the trabecular bone specimen presented in [107]. The geometry is shown in Figure 7, which also depicts the ambient domain of $(0\text{ mm}, 1.28\text{ mm})^3$. The Young's modulus is taken as $E = 10$ GPa and the Poisson's ratio is $\nu = 0.3$. The top boundary is constrained with a homogeneous Dirichlet condition, and at the bottom boundary a uniform displacement of 0.0128 mm in the vertical direction is applied, resulting in an average compression of 1%. To avoid the computational cost involved in determining the element-wise stabilization parameters, the Dirichlet conditions are applied by the penalty method instead of Nitsche's method. The weak formulation in (13) then reduces to

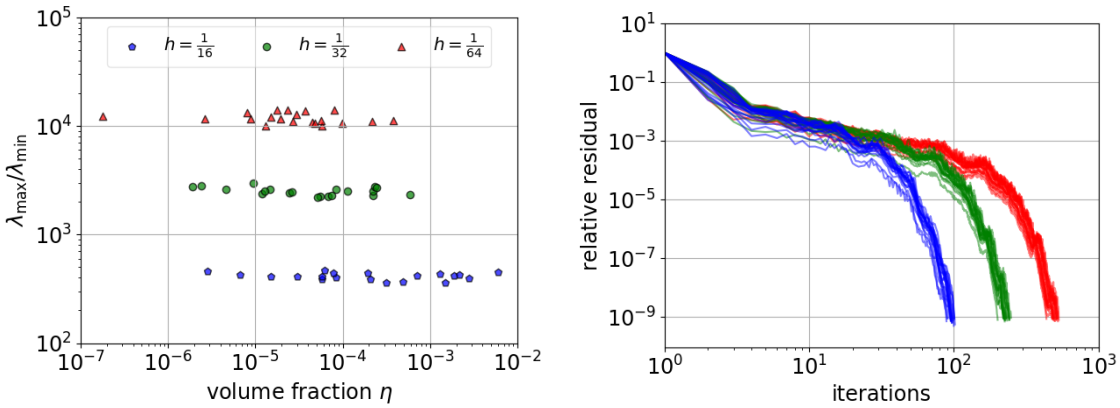

(a) Eigenvalue ratios

(b) Residual

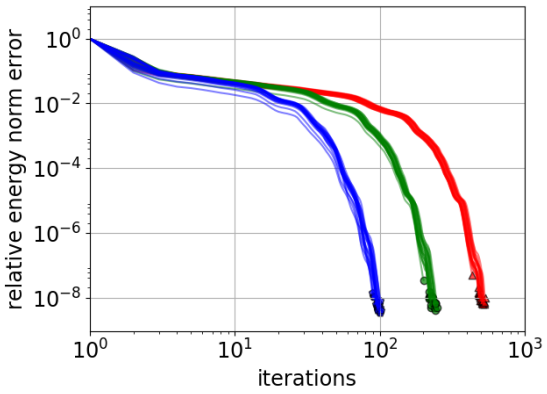

(c) Error in the energy norm

Figure 5: Investigation of the performance of the Additive-Schwarz preconditioner on grids of $h = \frac{1}{16}$, $h = \frac{1}{32}$, and $h = \frac{1}{64}$ using quadratic B-spline bases for the 2D elasticity problem.

$$\begin{cases} \text{Find } \boldsymbol{u}_h \in \mathcal{V}_h(\Omega) \text{ such that for all } \boldsymbol{v}_h \in \mathcal{V}_h(\Omega): \\ \\ \int_\Omega \nabla^s \boldsymbol{v}_h : \boldsymbol{\sigma}(\boldsymbol{u}_h)\,\mathrm{d}V + \int_{\Gamma^D} \lambda\beta^\lambda(\boldsymbol{v}_h \cdot \boldsymbol{n})(\boldsymbol{u}_h \cdot \boldsymbol{n}) + 2\mu\beta^\mu \boldsymbol{v}_h \cdot \boldsymbol{u}_h\,\mathrm{d}S \\ = \int_{\Gamma^D} \lambda\beta^\lambda(\boldsymbol{v}_h \cdot \boldsymbol{n})(\boldsymbol{g}^D \cdot \boldsymbol{n}) + 2\mu\beta^\mu \boldsymbol{v}_h \cdot \boldsymbol{g}^D\,\mathrm{d}S. \end{cases}$$

The penalty parameters are set to $\beta^\lambda = \beta^\mu = \frac{10}{h}$. The integration depth for the quadrature is set to 2 for the grids up to $64 \times 64 \times 64$ elements and to 0 for the finest grid of $128 \times 128 \times 128$ elements, in order to reduce the computation time. The solution depicted in Figure 7 is computed on a grid of $64 \times 64 \times 64$ elements with a quadratic B-spline basis.

Figure 8a reports the convergence of the relative residual in a Conjugate Gradient solver for different grid sizes. The number of iterations increases from 144 for the coarsest grid of $4 \times 4 \times 4$ elements to 9 360 for the finest grid of $128 \times 128 \times 128$ elements. The number of supported basis functions varies from 639 to 1 054 491. The observed behavior is similar to that of the two-dimensional problems in Figure 5b. The number of iterations increases with a factor slightly larger than 2 between the three finest grids. We expect this to be caused by the system changing from a regime where nearly all elements are cut and receive the Additive-Schwarz treatment to a regime where the majority of the basis functions is only diagonally scaled. Figure 8b depicts the CPU times to solve the system on a single core. The scaling of the CPU time derived in Section 3.3 is indicated by the dashed line, which conveys that the theoretical rate of $\mathcal{O}(h^{-(d+1)}) = \mathcal{O}(h^{-4})$ is closely followed.

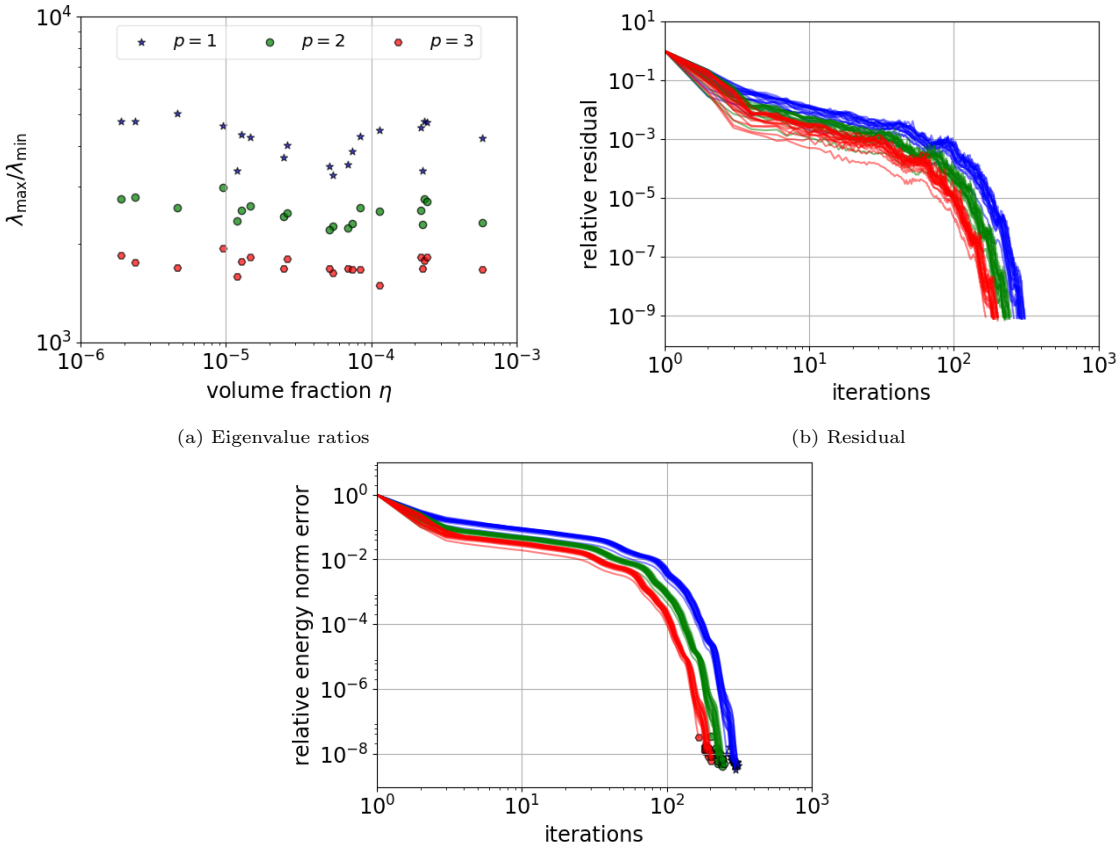

(a) Eigenvalue ratios

(b) Residual

(c) Error in the energy norm

Figure 6: Investigation of the performance of the Additive-Schwarz preconditioner on a grid of $h = \frac{1}{32}$ with optimal regularity B-spline bases of orders $p = 1$, $p = 2$, and $p = 3$ for the 2D elasticity problem.

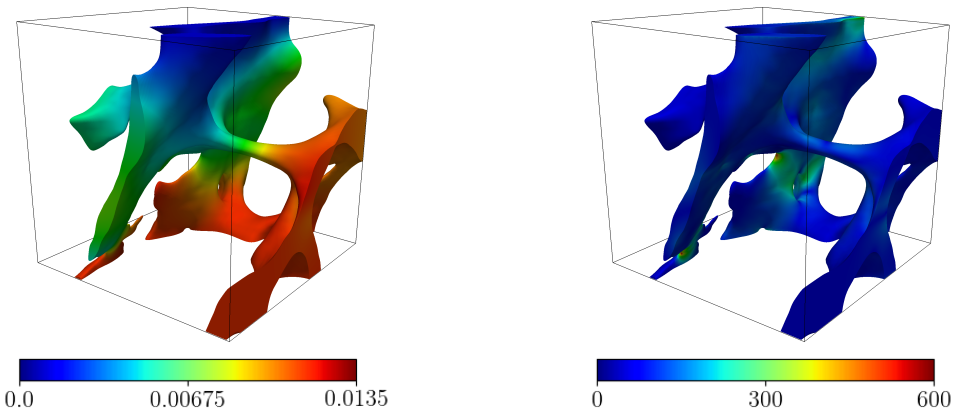

(a) Displacement magnitude [mm]

(b) Frobenius norm of stress tensor [MPa]

Figure 7: Domain and solution of the elasticity problem on the three-dimensional trabecular bone geometry with a grid of $64 \times 64 \times 64$ elements.

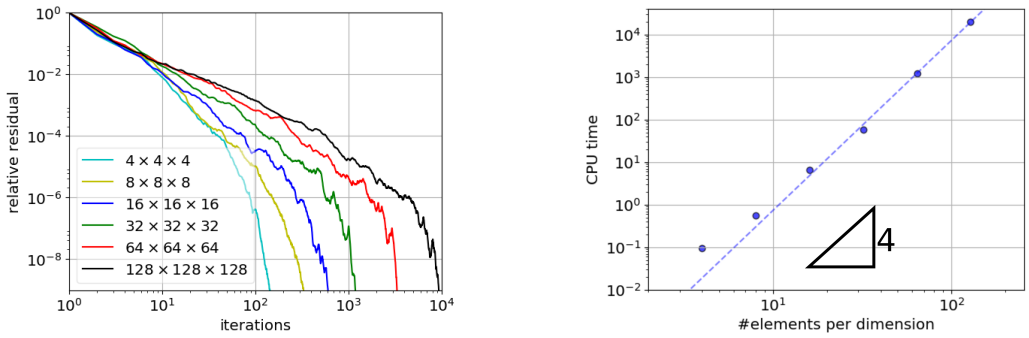

(a) Convergence (b) CPU time

Figure 8: Convergence of the relative preconditioned residual with the Conjugate Gradient solver and CPU times for the three-dimensional elasticity problem with different grid sizes.

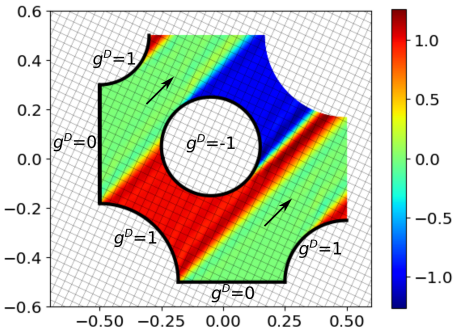

Figure 9: Boundary conditions and solution of the convection-diffusion problem in (16). The Dirichlet boundary Γ^D is indicated by the thick black lines and the arrow indicates the direction of the convective velocity $\boldsymbol{w}$. Note that the convection causes slight oscillations in the solution, which we ignore as we focus on the conditioning and iterative solution of the linear system.

4.2. Convection-diffusion problems

We consider the convection-dominated convection-diffusion problem

$$\begin{cases} \operatorname{div}(\boldsymbol{w}u - \varepsilon\nabla u) = 0 & \text{in } \Omega, \\ u = g^D & \text{on } \Gamma^D, \\ \varepsilon\partial_n u - \frac{1}{2}\min(0, \boldsymbol{w}\cdot\boldsymbol{n})\, u = g^N = 0 & \text{on } \Gamma^N, \end{cases} \tag{16}$$

with scalar solution variable u, dimensionless convective velocity $\boldsymbol{w} = (1, 1)$, dimensionless diffusion coefficient $0 < \varepsilon = 10^{-6} \ll 1$ such that $|\boldsymbol{w}| \gg \varepsilon$, and $\partial_n = \boldsymbol{n}\cdot\nabla$ denoting the co-normal derivative. A directional do-nothing term is included in the Neumann condition to ensure the problem is well posed in case of inflow through the Neumann boundary Γ^N [111–113]. The boundary conditions and the solution using a quadratic B-spline basis with grid size $h = \frac{1}{32}$ at an angle $\theta = 22.5^\circ$ are presented in Figure 9.

We employ a weak form in which the convective terms are formulated skew-symmetrically as in [113, 114] and stabilized by Streamline Upwind/Petrov-Galerkin (SUPG) terms [100]. Boundary conditions are enforced by Nitsche's method with an additional penalty scaling with the inflow velocity as proposed in [115]. The weak form reads

$$
\begin{cases}
\text{Find } u_h \in \mathcal{V}_h(\Omega) \text{ such that for all } v_h \in \mathcal{V}_h(\Omega): \\
\\
\int_\Omega \frac{1}{2} v_h \boldsymbol{w} \cdot \nabla u_h - \frac{1}{2} u_h \boldsymbol{w} \cdot \nabla v_h + \varepsilon \nabla v_h \cdot \nabla u_h + \tau \boldsymbol{w} \cdot \nabla v_h \mathrm{div}\left(\boldsymbol{w} u_h - \varepsilon \nabla u_h\right) \mathrm{d}V \\
\quad + \int_{\partial\Omega} \frac{1}{2} \max\left(0, \boldsymbol{w} \cdot \boldsymbol{n}\right) v_h u_h \,\mathrm{d}S + \varepsilon \int_{\Gamma^D} -v_h \partial_n u_h - u_h \partial_n v_h + \beta v_h u_h \,\mathrm{d}S \\
\\
= \int_{\Gamma^D} -\frac{1}{2} \min\left(0, \boldsymbol{w} \cdot \boldsymbol{n}\right) v_h g^D \,\mathrm{d}S + \varepsilon \int_{\Gamma^D} -g^D \partial_n v_h + \beta v_h g^D \,\mathrm{d}S.
\end{cases}
\tag{17}
$$

For this scalar problem the element-wise stabilization parameter is defined as

$$
\beta|_{K_i} = 2 \max_{v_h \in \mathcal{V}_h(K_i)} \frac{\|\partial_n v_h\|^2_{L^2(B_i^D)}}{\|\nabla v_h\|^2_{L^2(K_i^{\mathrm{tr}})}}, \tag{18}
$$

which can again be computed by the approach described in [77]. Different choices for the SUPG parameter τ are motivated in [116]. In all our examples we use $\tau = h^* / \left(2|\boldsymbol{w}|\right)$ with h^* the maximal element length in the direction of velocity $\boldsymbol{w}$. For uniform tensor product grids this implies $\tau = h / \left(2 \max_i \left(|\boldsymbol{w} \cdot \boldsymbol{e}_i|\right)\right)$, with $\boldsymbol{e}_i$ the unit vector in the direction of a grid line. We therefore have

$$
\tau = \frac{h}{2\sqrt{2} \sin\left(\frac{1}{4}\pi + \theta\right)}. \tag{19}
$$

Our computations based on τ according to (19) as a global parameter did not indicate a need to consider a typical length scale $\hat{h}^*_{K_i^{\mathrm{tr}}}$ of a trimmed element. We did not perform an in depth investigation of this aspect however, and cannot assert that this observation holds generally.

The performance of the Additive-Schwarz preconditioner is compared to a Jacobi preconditioner in Figure 10. We again consider the linear systems for all grid angles θ with a grid size $h = \frac{1}{32}$ using quadratic B-splines, yielding approximately 900 degrees of freedom. Figure 10a shows the ratios between the largest and smallest eigenvalues, plotted against the smallest volume fractions η. It is noted that the eigenvalue ratios with Jacobi preconditioning are very similar to those of the elasticity problem in Figure 4a, which indicates that the conditioning problems are the result of how elements are cut and that the considered partial differential equation and boundary conditions play a minor role. Figure 10b plots the convergence of the relative preconditioned residual in a GMRES solver that is terminated at a reduction of 2^{-30}. The preconditioned residual is a value that is naturally computed in a GMRES solver. The figure demonstrates that the Additive-Schwarz preconditioner is robust with respect to the rotation angle with iteration counts ranging between 90 and 130. We expect that the minor variation in the number of iterations between approximately 90 and 130 for the preconditioned solver is caused by variation in the (mis)alignment between the convective velocity and the grid lines and consequently the variation in the value of stabilization parameter τ. The Jacobi preconditioner is not robust to how elements are cut, and for certain rotations the iteration count increases to more than 400.

Figure 11 investigates the effect of the grid size and discretization order on the performance of the preconditioner. Figure 11a conveys that the behavior of the GMRES solver is robust for all grid sizes, and that the observed numbers of iterations show a similar dependence on the grid size as the Conjugate Gradient solver for the elasticity problem. The systems corresponding to different grid sizes comprise approximately 300, 900 and 3 200 degrees of freedom. Figure 11b shows that Additive-Schwarz preconditioned GMRES is robust to the different discretization orders. Again the convergence demonstrates a minor dependence on the order, where for this problem the convergence of the lower orders is faster than for the higher orders. The discretization orders $p = 1, 2, 3$ carry approximately 800, 900, and 1 000 degrees of freedom, respectively.

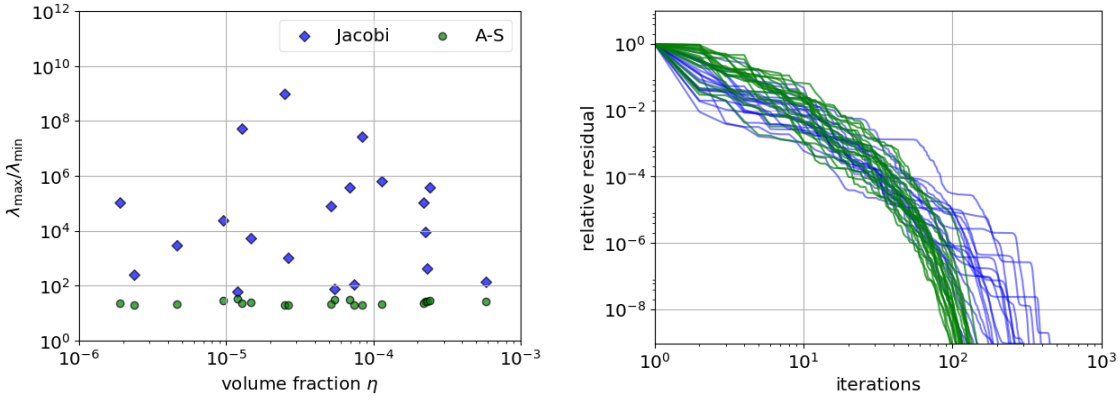

(a) Eigenvalue ratios

(b) Residual

Figure 10: Comparison of the Additive-Schwarz and Jacobi preconditioner with grids of $h = \frac{1}{32}$ using quadratic B-spline bases for the 2D convection-diffusion problem.

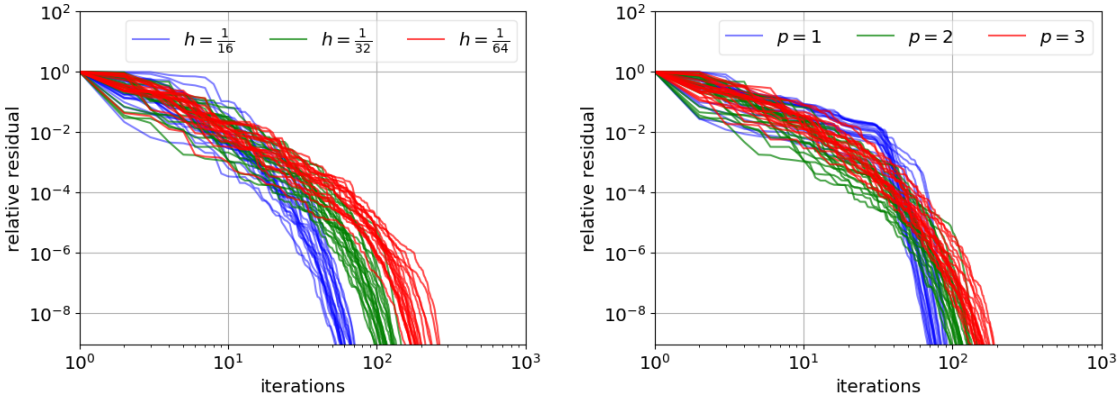

(a) Grid size

(b) Discretization order

Figure 11: Investigation of the effect of the grid size and discretization order on the performance of the Additive-Schwarz preconditioner for the convection-diffusion problem. Figure (a) displays the convergence with grids of $h = \frac{1}{16}$, $h = \frac{1}{32}$, and $h = \frac{1}{64}$ using quadratic B-spline bases. Figure (b) displays the convergence on a grid of $h = \frac{1}{32}$ using optimal regularity B-spline bases of orders $p = 1$, $p = 2$, and $p = 3$.

4.3. Incompressible Stokes flow problems

We consider the incompressible Stokes flow problem in dimensionless form

$$\begin{cases} \operatorname{div}(2\nabla^s \boldsymbol{u} - p\mathbf{I}) = \mathbf{0} & \text{in } \Omega, \\ \operatorname{div}(\boldsymbol{u}) = 0 & \text{in } \Omega, \\ \boldsymbol{u} = \boldsymbol{g}^D & \text{on } \Gamma^D, \\ (2\nabla^s \boldsymbol{u} - p\mathbf{I})\,\boldsymbol{n} = \boldsymbol{g}^N & \text{on } \Gamma^N, \end{cases} \tag{20}$$

on the domain in Figure 12. In this formulation $\boldsymbol{u}$ and p denote the velocity and the pressure, respectively. The leftmost boundary of the domain is the inflow boundary where we impose a Neumann condition with a uniform normal traction. The rightmost boundary is the outflow boundary and is traction free. On all other boundaries homogeneous Dirichlet, i.e., no-slip, boundary conditions are imposed. The boundary conditions and the solution with a quadratic Taylor-Hood basis on a grid of $h = \frac{1}{32}$ at an angle of 22.5° are shown in Figure 12.

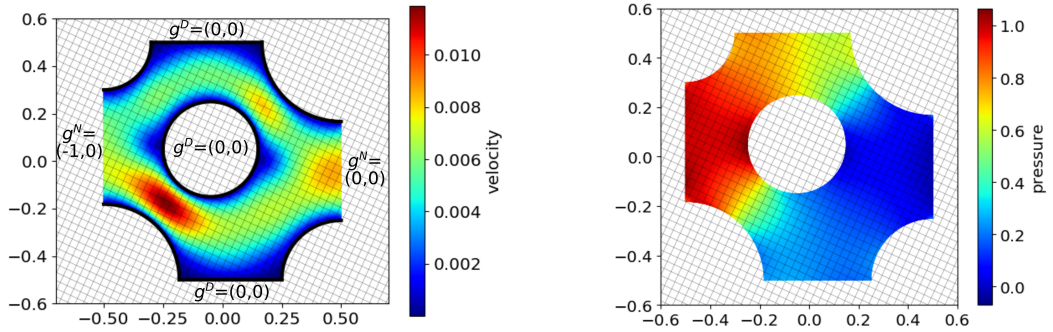

(a) Velocity magnitude

(b) Pressure

Figure 12: Boundary conditions and solution to the 2D Stokes flow problem. The leftmost inflow boundary contains a uniform normal traction Neumann condition, the rightmost outflow boundary contains a traction free Neumann condition, the other boundaries contain no-slip Dirichlet conditions indicated by the thick black lines in (a).

The symmetric variational form with boundary conditions imposed by Nitsche's method is

$$\begin{cases} \text{Find } (\boldsymbol{u}_h, p_h) \in \mathcal{V}_h(\Omega) \times \mathcal{Q}_h(\Omega) \text{ such that for all } (\boldsymbol{v}_h, q_h) \in \mathcal{V}_h(\Omega) \times \mathcal{Q}_h(\Omega): \\ \int_\Omega 2\nabla^s \boldsymbol{v}_h : \nabla^s \boldsymbol{u}_h \,\mathrm{d}V + \int_{\Gamma^D} -2\boldsymbol{v}_h \cdot (\nabla^s \boldsymbol{u}_h)\boldsymbol{n} - 2\boldsymbol{u}_h \cdot (\nabla^s \boldsymbol{v}_h)\boldsymbol{n} + 2\beta \boldsymbol{v}_h \cdot \boldsymbol{u}_h \,\mathrm{d}S \\ \quad + \int_\Omega -p_h \mathrm{div}\,(\boldsymbol{v}_h) - q_h \mathrm{div}\,(\boldsymbol{u}_h) \,\mathrm{d}V + \int_{\Gamma^D} p_h \boldsymbol{v}_h \cdot \boldsymbol{n} + q_h \boldsymbol{u}_h \cdot \boldsymbol{n} \,\mathrm{d}S \\ = \int_{\Gamma^N} \boldsymbol{v}_h \cdot \boldsymbol{g}^N \,\mathrm{d}S + \int_{\Gamma^D} -2\boldsymbol{g}^D \cdot (\nabla^s \boldsymbol{v}_h)\boldsymbol{n} + 2\beta \boldsymbol{v}_h \cdot \boldsymbol{g}^D + q_h \boldsymbol{g}^D \cdot \boldsymbol{n} \,\mathrm{d}S. \end{cases} \tag{21}$$

The element-wise stabilization constant β in this formulation is equal to β^μ in (15). In order to obtain an inf-sup stable formulation, a proper choice for the pair of spaces $\mathcal{V}_h(\Omega)$ and $\mathcal{Q}_h(\Omega)$ is needed. An analysis of the inf-sup stability and performance of different pairs of function spaces and formulations for immersed finite element methods can be found in [117, 118]. We apply a Taylor-Hood pair that comprises a $\mathcal{N}^p_{p-2}(\mathcal{T}^h)$ B-spline basis for $\mathcal{V}_h$ and a $\mathcal{N}^{p-1}_{p-2}(\mathcal{T}^h)$ B-spline basis for $\mathcal{Q}_h$, with p denoting the order of the discretization.

The performance of the Additive-Schwarz preconditioner and the Jacobi preconditioner is reported in Figure 13. The preconditioners for the velocity are based on the velocity matrix and the preconditioners for the pressure are based on the pressure mass matrix, which serves as an approximate Schur complement as discussed in Section 3.1. For all grid angles θ the linear systems are computed for a quadratic, $p = 2$, basis on a grid with $h = \frac{1}{32}$, resulting in approximately 7 100 degrees of freedom. The eigenvalue ratios of the symmetric systems in Figure 13a are similar to the eigenvalue ratios of the elasticity problem and the convection-diffusion problem. This demonstrates that the effectiveness of Jacobi preconditioning depends on how the elements are cut, while the Additive-Schwarz preconditioner is uniformly effective for all configurations. Figure 13b shows the convergence of the preconditioned residual with a GMRES solver, that is terminated at a residual of 2^{-30} or when the number of iterations exceeds 2 500. One can observe that the Additive-Schwarz preconditioner is robust and behaves uniformly for all configurations. Jacobi-preconditioned GMRES generally converges slower than Additive-Schwarz-preconditioned GMRES. For approximately half of the considered angles, Jacobi-preconditioned GMRES does not achieve convergence within the prescribed maximum number of iterations. Let us note that by virtue of the symmetry of the Stokes problem, we could have sufficed with MINRES instead of GMRES. However, we have opted for the use of the generally applicable GMRES to retain uniformity in the presentation.

The effect of the grid size and the order of the discretization is investigated in Figure 14. The convergence of the preconditioned residual with the GMRES solver in Figure 14a demonstrates that the Additive-Schwarz preconditioner is uniformly effective for the different grid sizes. The observed

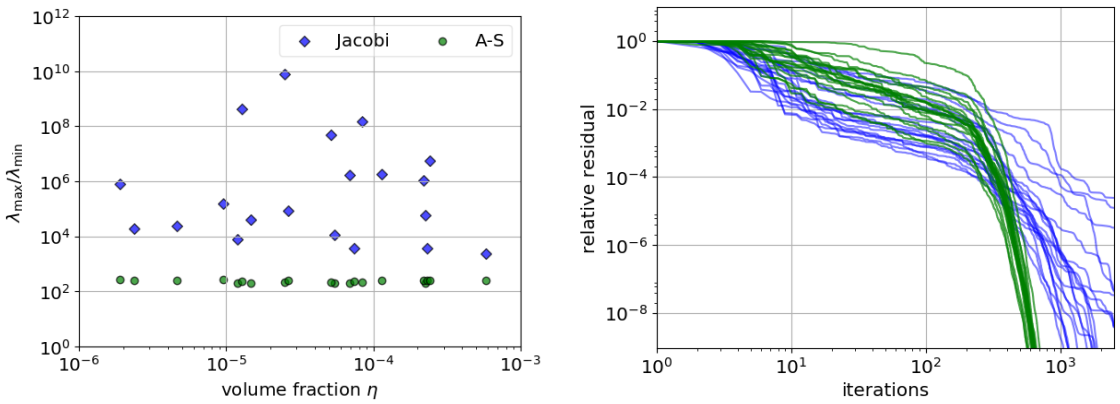

(a) Eigenvalue ratios

(b) Residual convergence

Figure 13: Comparison of the effectiveness of the Additive-Schwarz and Jacobi preconditioner for the 2D Stokes problem with grids of $h = \frac{1}{32}$ and a discretization order of $p = 2$.

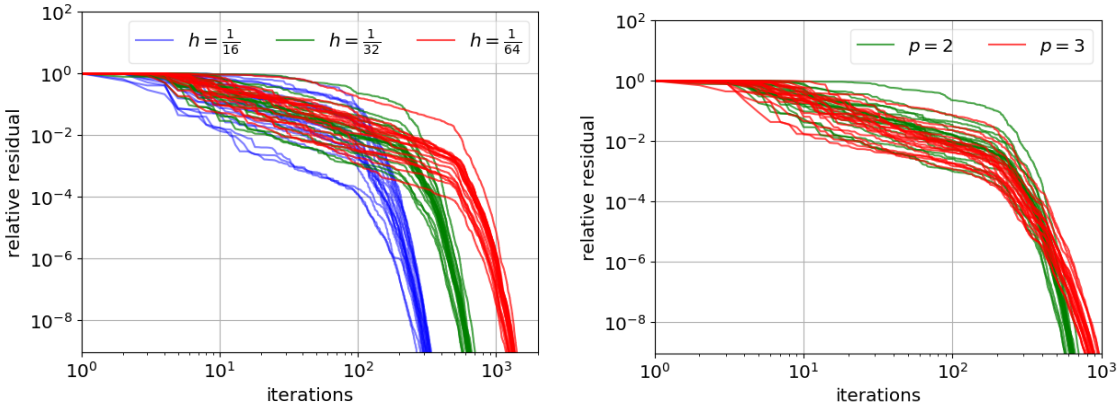

(a) Grid size

(b) Discretization order

Figure 14: Convergence of the preconditioned residual of the 2D Stokes problem. Figure (a) displays different grid sizes with $p = 2$. Figure (b) displays discretization order $p = 2$ and $p = 3$ with a grid of $h = \frac{1}{32}$.

numbers of iterations are approximately inversely proportional to the mesh size, which was also observed for the elasticity problem and the convection-diffusion problem. The systems with the different grid sizes have approximately 2 100, 7 100 and 25 700 degrees of freedom. Figure 14b shows that the preconditioner is effective for both $p = 2$ and $p = 3$, where the cubic space requires slightly more iterations than the quadratic space. The systems have approximately 7 100 and 7 600 degrees of freedom for the different systems.

Next, we consider the properties of the Additive-Schwarz preconditioning scheme for a three-dimensional Stokes flow around the popcorn flake introduced in [119] reduced in size by a factor 2. The domain consists of the bi-unit cube, with the popcorn flake excluded at the center. At the left boundary, $x_1 = -1$, we prescribe a parabolic inflow velocity normal to the boundary with dimensionless maximum velocity 1, i.e., we impose the Dirichlet condition $\boldsymbol{g}^D = ((1 - x_2^2)(1 - x_3^2), 0, 0)$. The right boundary, $x_1 = 1$, is a homogeneous Neumann outflow boundary. On all other boundaries no-slip Dirichlet conditions are imposed. To reduce the computational cost we apply a penalty method instead of Nitsche's method, such that we do not have to compute the element-wise stabilization parameters. We therefore set $\beta = \frac{10}{h}$ and remove the viscous terms on the Dirichlet boundary from the variational formulation

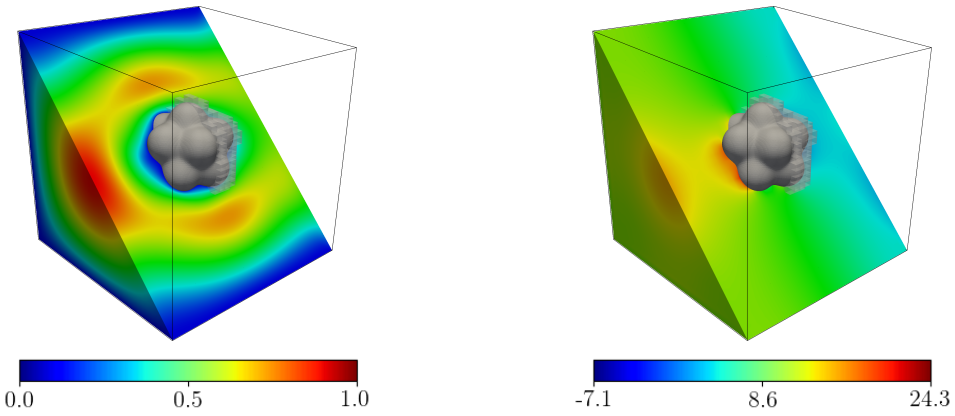

(a) Velocity magnitude (b) Pressure

Figure 15: Domain and solution of the three-dimensional Stokes flow around the popcorn flake with a grid of $32 \times 32 \times 32$ elements and a quadratic Taylor-Hood basis.

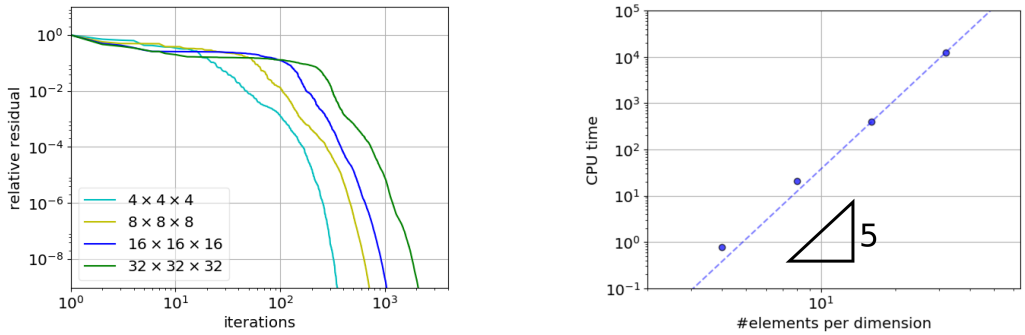

(a) Convergence (b) CPU time

Figure 16: Convergence of the relative preconditioned residual with GMRES (a) and CPU times (b) for the three-dimensional Stokes problem with different grid sizes.

$$
\begin{cases}
\text{Find } (\boldsymbol{u}_h, p_h) \in \mathcal{V}_h(\Omega) \times \mathcal{Q}_h(\Omega) \text{ such that for all } (\boldsymbol{v}_h, q_h) \in \mathcal{V}_h(\Omega) \times \mathcal{Q}_h(\Omega): \\
\int_\Omega 2\nabla^s \boldsymbol{v}_h : \nabla^s \boldsymbol{u}_h - p_h \mathrm{div}\,(\boldsymbol{v}_h) - q_h \mathrm{div}\,(\boldsymbol{u}_h)\, \mathrm{d}V + \int_{\Gamma^D} 2\beta \boldsymbol{v}_h \cdot \boldsymbol{u}_h + p_h \boldsymbol{v}_h \cdot \boldsymbol{n} + q_h \boldsymbol{u}_h \cdot \boldsymbol{n}\, \mathrm{d}S \\
= \int_{\Gamma^N} \boldsymbol{v}_h \cdot \boldsymbol{g}^N\, \mathrm{d}S + \int_{\Gamma^D} 2\beta \boldsymbol{v}_h \cdot \boldsymbol{g}^D + q_h \boldsymbol{g}^D \cdot \boldsymbol{n}\, \mathrm{d}S.
\end{cases}
$$

Similar to the three-dimensional elasticity problem, the integration depth is set to 2. The domain and the solution on a $32 \times 32 \times 32$ grid with a quadratic Taylor-Hood basis are displayed in Figure 15.

The convergence of a GMRES solver with the dedicated Additive-Schwarz preconditioner for different grid sizes with quadratic Taylor-Hood bases is shown in Figure 16a. The systems contain 2 312, 15 468, 112 216, and 848 012 degrees of freedom, respectively. The convergence plots are similar to those for the different grid sizes for the two-dimensional problems in Figure 14a. The increase in the number of iterations between the $8 \times 8 \times 8$ and the $16 \times 16 \times 16$ grid is slightly less than the expected factor 2, which we attribute to pre-asymptotic behavior. The CPU time for the GMRES solver on a single core is reported in Figure 16b. The dashed line depicts the scaling rate that is estimated in Section 3.3, which is observed to be in excellent agreement.

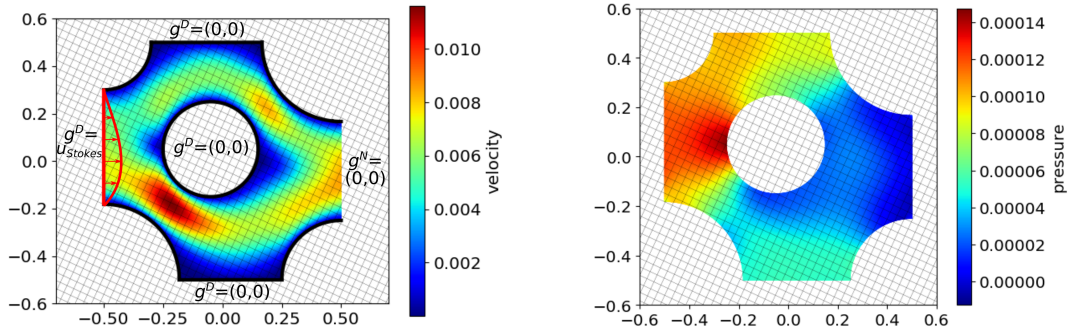

(a) Velocity magnitude

(b) Pressure

Figure 17: Boundary conditions and solution of the 2D Navier-Stokes problem with $\nu = 10^{-4}$ (Re $\approx$ 25). The thick lines in Figure (a) indicate the Dirichlet boundary, with the solution to the Stokes problem as the inflow condition at the leftmost boundary and no-slip conditions at all other Dirichlet boundaries.

4.4. Steady incompressible Navier-Stokes flow problems

To solve the steady Navier-Stokes equations we first consider the Oseen problem

$$\begin{cases} \operatorname{div}(\boldsymbol{w} \otimes \boldsymbol{u} - 2\nu\nabla^s\boldsymbol{u} + p\mathbf{I}) = \mathbf{0} & \text{in } \Omega, \\ \operatorname{div}(\boldsymbol{u}) = 0 & \text{in } \Omega, \\ \boldsymbol{u} = \boldsymbol{g}^D & \text{on } \Gamma^D, \\ (2\nu\nabla^s\boldsymbol{u} - p\mathbf{I})\,\boldsymbol{n} - \frac{1}{2}\min(0, \boldsymbol{w}\cdot\boldsymbol{n})\,\boldsymbol{u} = \boldsymbol{g}^N & \text{on } \Gamma^N, \end{cases} \tag{22}$$

with divergence free convection velocity $\boldsymbol{w}$. Note the directional do-nothing term in the Neumann boundary condition to ensure well-posedness in case of backflow through Γ^N [111–113], *cf.* the convection-diffusion problem in Section 4.2. The nonlinear steady Navier-Stokes equations are obtained by replacing the convection velocity $\boldsymbol{w}$ with $\boldsymbol{u}$. We solve this system by means of a standard Picard iteration procedure, in which the Oseen problem is successively solved with at the i^{th} iteration the convection velocity set to $\boldsymbol{w} = \boldsymbol{u}^{i-1}$. The initial convection velocity is set to $\boldsymbol{w} = \mathbf{0}$, such that in the first iteration the Stokes problem is solved. The applied stopping criterion is

$$\sqrt{\frac{\|\boldsymbol{u}^i - \boldsymbol{u}^{i-1}\|^2_{H^1(\Omega)} + \|p^i - p^{i-1}\|^2_{L^2(\Omega)}}{\|\boldsymbol{u}^i + \boldsymbol{u}^{i-1}\|^2_{H^1(\Omega)} + \|p^i + p^{i-1}\|^2_{L^2(\Omega)}}} \leq \text{tol} = 10^{-4}.$$

The dimensionless kinematic viscosity is set to $\nu = 10^{-4}$. We use the solution to the Stokes problem in (20) as a Dirichlet inflow boundary condition at the leftmost boundary, and apply the same boundary conditions as the Stokes problem for the other boundaries. The full set of boundary conditions and the solution are shown in Figure 17, with a quadratic Taylor-Hood basis on a grid with $h = \frac{1}{32}$ at an angle of 22.5°. The resulting Reynolds number is approximately 25.

The considered weak form for the Oseen equations is based on the skew symmetric convection formulation [113, 114] with additional penalization on the Dirichlet boundaries with the inflow velocity as in [115]:

$$\begin{cases} \text{Find } (\boldsymbol{u}_h, p_h) \in \mathcal{V}_h(\Omega) \times \mathcal{Q}_h(\Omega) \text{ such that for all } (\boldsymbol{v}_h, q_h) \in \mathcal{V}_h(\Omega) \times \mathcal{Q}_h(\Omega): \\ \\ \int_\Omega 2\nu\nabla^s\boldsymbol{v}_h : \nabla^s\boldsymbol{u}_h \,\mathrm{d}V + \int_{\Gamma^D} -2\nu\boldsymbol{v}_h\cdot(\nabla^s\boldsymbol{u}_h)\boldsymbol{n} - 2\nu\boldsymbol{u}_h\cdot(\nabla^s\boldsymbol{v}_h)\boldsymbol{n} + 2\beta\nu\boldsymbol{v}_h\cdot\boldsymbol{u}_h \,\mathrm{d}S \\ \quad + \int_\Omega \frac{1}{2}\boldsymbol{v}_h\cdot(\nabla\boldsymbol{u}_h)\boldsymbol{w} - \frac{1}{2}\boldsymbol{u}_h\cdot(\nabla\boldsymbol{v}_h)\boldsymbol{w} \,\mathrm{d}V + \int_{\partial\Omega}\frac{1}{2}\max(0, \boldsymbol{w}\cdot\boldsymbol{n})\,\boldsymbol{v}_h\cdot\boldsymbol{u}_h \,\mathrm{d}S \\ \quad + \int_\Omega -p_h\operatorname{div}(\boldsymbol{v}_h) - q_h\operatorname{div}(\boldsymbol{u}_h) \,\mathrm{d}V + \int_{\Gamma^D} p_h\boldsymbol{v}_h\cdot\boldsymbol{n} + q_h\boldsymbol{u}_h\cdot\boldsymbol{n} \,\mathrm{d}S \\ \\ = \int_{\Gamma^D} -2\nu\boldsymbol{g}^D\cdot(\nabla^s\boldsymbol{v}_h)\boldsymbol{n} + 2\beta\nu\boldsymbol{v}_h\cdot\boldsymbol{g}^D - \frac{1}{2}\min(0, \boldsymbol{w}\cdot\boldsymbol{n})\,\boldsymbol{v}_h\cdot\boldsymbol{g}^D + q_h\boldsymbol{g}^D\cdot\boldsymbol{n} \,\mathrm{d}S \\ \quad + \int_{\Gamma^N}\boldsymbol{v}_h\cdot\boldsymbol{g}^N \,\mathrm{d}S \end{cases} \tag{23}$$

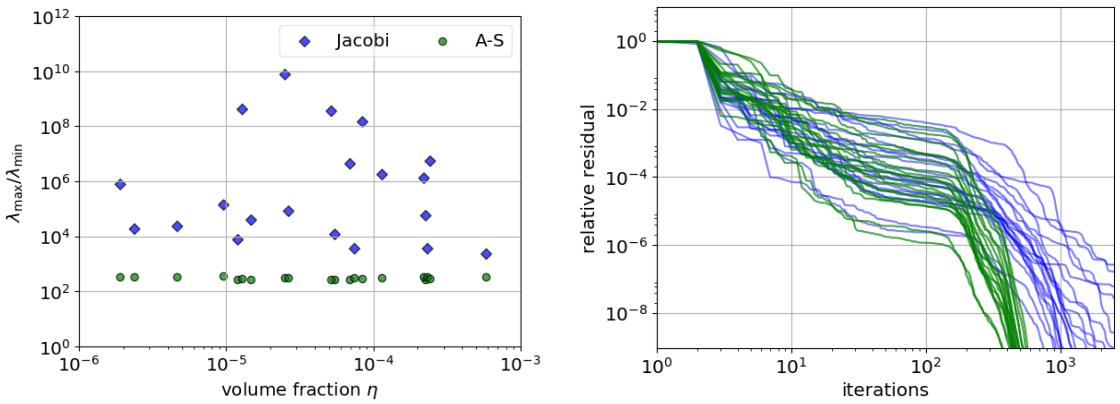

(a) Eigenvalue ratios

(b) Residual convergence

Figure 18: Comparison of the Additive-Schwarz preconditioner and Jacobi preconditioner for the 2D Navier-Stokes problem with grids of $h = \frac{1}{32}$ and a discretization order of $p = 2$.

Similar formulations can be found in [3, 15–18, 21–23, 25–27, 120, 121]. The variational forms in most of these references contain Variational MultiScale (VMS) stabilization terms to enhance stability for large convective velocities [101–103]. The two-dimensional and three-dimensional examples presented in this manuscript with both a Reynolds number of approximately 25 did not require this stabilization. Furthermore, these stabilization terms have originally been developed for linear bases and have in the context of immersed finite element methods only been used with such linear bases [15–17], with a stabilization parameter that is decreased in the vicinity of the trimmed elements [3, 21, 27] or in combination with additional stabilization techniques such as ghost penalty terms on trimmed elements [22–26].

The system matrix and consequently the conditioning depend on the convective velocity $\boldsymbol{w}$. Because the convective velocity changes in the Picard iterations, so does the system matrix and, hence, its condition number. To keep our report of the results concise, we only present the eigenvalue ratios and the convergence of the GMRES solver with the converged convective velocity. We have observed that the convective velocity does not significantly affect the conditioning. Similar to the Stokes problem, the pressure space is preconditioned using the pressure mass matrix as an approximate Schur complement.

The Additive-Schwarz preconditioner is compared to a Jacobi preconditioner for quadratic bases with a grid size of $h = \frac{1}{32}$ in Figure 18. All the systems contain approximately 7 100 degrees of freedom. One can observe that the results are very similar to those of the Stokes problem in Figure 13. The convergence of the GMRES solver for the different angles is less uniform for Navier-Stokes than for Stokes. We conjecture that these non-uniformities are caused by the (mis)alignment of the background grid lines with the convection velocity, similar to the convection-diffusion problem.

In Figure 19 the effect of the grid size and the discretization order on the Additive-Schwarz preconditioner is reported. Figure 19a contains the convergence of the GMRES solver for the preconditioned residual on grids with $h = \frac{1}{16}$, $h = \frac{1}{32}$, and $h = \frac{1}{64}$, resulting in systems of approximately 2 100, 7 100 and 25 700 degrees of freedom, respectively. The results are again very similar to those of the Stokes problem, with a larger spread in the iteration counts, which we again attribute to the (mis)alignment between the convection velocity and the grid lines. Figure 19b investigates the effect of the discretization order on a grid with $h = \frac{1}{32}$. The systems for $p = 2$ and $p = 3$ contain approximately 7 100 and 7 600 degrees of freedom, respectively. These results are similar to those of the Stokes problem, with again slightly more spreading in the iteration counts.

To elucidate the properties of the Additive-Schwarz preconditioner for a 3D Navier-Stokes problem, we consider the same three-dimensional popcorn flake problem as for the Stokes problem. We again replace Nitsche's method in the weak form by the penalty method, in the same way as

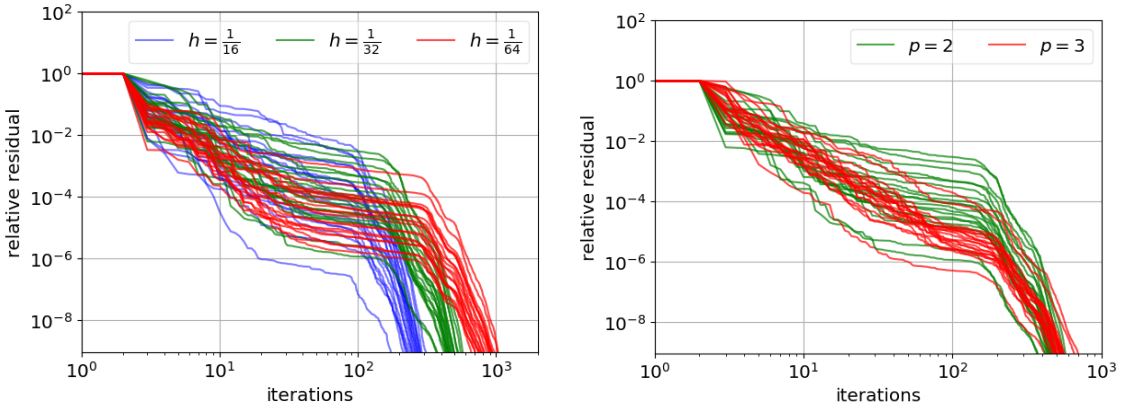

(a) Grid size

(b) Discretization order

Figure 19: Convergence of the preconditioned residual at the last Picard iteration of the 2D Navier-Stokes problem. Figure (a) displays different grid sizes with $p = 2$. Figure (b) displays discretization orders $p = 2$ and $p = 3$ with a grid of $h = \frac{1}{32}$.

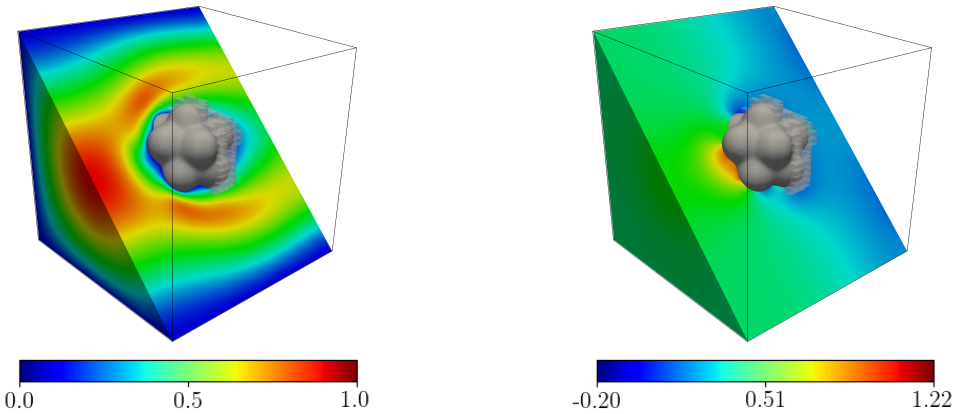

(a) Velocity magnitude

(b) Pressure

Figure 20: Solution to the three-dimensional Navier-Stokes flow around the popcorn flake with a grid of $32 \times 32 \times 32$ elements and a quadratic Taylor-Hood basis.

for the three-dimensional Stokes problem. We set the dimensionless kinematic viscosity to $\nu = \frac{1}{35}$. With the maximum inflow velocity of 1 and the diameter of the popcorn flake of approximately 0.71, this results in a Reynolds number of approximately 25. The solution is shown in Figure 20.

The convergence of a GMRES solver with the Additive-Schwarz preconditioner for different grid sizes with quadratic Taylor-Hood bases is shown in Figure 21. The systems again contain 2 312, 15 468, 112 216, and 848 012 degrees of freedom, respectively. The behavior is similar to that of the three-dimensional Stokes problem in Figure 16a and the two-dimensional Navier-Stokes problems in Figure 19a. It is observed that on the finest grid the solution converges to approximately $1.1 \cdot 10^{-9}$ and does not achieve the full tolerance of 2^{-30}. This is the result of round-off errors that cause a failure in the orthogonalization of the vectors that span the Krylov space in GMRES, as described in Remark 3.3. We have resolved this by applying a restart after 2 000 iterations in the GMRES algorithm (illustrated in the figure by the dashed line). Alternatively, this issue can be resolved by weakening the threshold at which basis functions are eliminated (not reported in the figure).

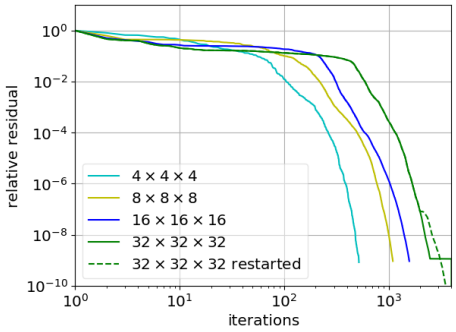

Figure 21: Convergence of the relative preconditioned residual of the GMRES solver for the three-dimensional Stokes problem on different grid sizes.

5. Concluding remarks

Motivated by the unavailability of versatile preconditioning techniques for immersed finite element problems, an Additive-Schwarz-type preconditioner is proposed that opens the door to higher-order immersed discretizations of a general class of flow problems. The proposed preconditioner derives its effectiveness from a tailored selection of the Additive-Schwarz blocks, which in essence combines diagonal scaling of untrimmed basis functions with element-wise inverses for trimmed basis functions. The performance of the preconditioner is demonstrated for a broad class of problems in both two and three dimensions, which convey that the cut-element related ill-conditioning problem is adequately resolved. In contrast to Jacobi preconditioning, the proposed preconditioner is robust with respect to the element size of the ambient mesh, the order of the discretization, the smoothness of the discretization, and the shape of the cut-elements.

Theoretical cost estimates for the considered preconditioned iterative solvers convey that, both in terms of floating point operations and in terms of memory usage, the proposed technique scales favorably compared to a direct solver. These estimates have been confirmed in our three-dimensional numerical simulations, which can be solved efficiently using the proposed preconditioner. The structure of vector-valued and mixed problems is leveraged in the Additive-Schwarz block selection to enhance the efficiency of the preconditioning technique. Application of the proposed technique to singular blocks in mixed systems (such as the pressure block in (Navier-)Stokes problems) is possible through an approximation of the Schur complement.

The exhibited behavior of the preconditioned systems is in close correspondence with characteristic behavior of mesh-fitting methods. This observation is evident, as untrimmed basis functions are treated straightforwardly by a Jacobi preconditioner. Consequently, the convergence of iterative solvers is still affected by aspects such as the discretization order and the mesh size in the usual manner as it does for mesh-fitting approaches. Especially the dependence of the convergence of the iterative solvers on the mesh size is apparent. It is therefore worthwhile to investigate the combination of the dedicated treatment of cut elements with existing preconditioning techniques, specifically multigrid techniques, to develop a method that is robust to a combination of the above mentioned effects.

Acknowledgement

The research of F. de Prenter was funded by NWO under the Graduate Program Fluid & Solid Mechanics. All simulations in this work were performed using the open source software package Nutils ([122], www.nutils.org). The code to construct the preconditioner and data to reproduce the results can be downloaded from https://gitlab.com/fritsdeprenter/additive-schwarz-immersed-fem. We would like to acknowledge fruitful discussions with Christoph Lehrenfeld regarding Additive-Schwarz preconditioning.

References

[1] J. Parvizian, A. Düster, E. Rank, Finite cell method, Computational Mechanics 41 (1) (2007) 121–133.

[2] E. Burman, S. Claus, P. Hansbo, M. Larson, A. Massing, CutFEM: Discretizing geometry and partial differential equations, International Journal for Numerical Methods in Engineering 104 (7) (2015) 472–501.

[3] D. Kamensky, M.-C. Hsu, D. Schillinger, J. Evans, A. Aggarwal, Y. Bazilevs, M. Sacks, T. Hughes, An immersogeometric variational framework for fluid–structure interaction: Application to bioprosthetic heart valves, Computer Methods in Applied Mechanics and Engineering 284 (2015) 1005–1053.

[4] T. Hughes, J. Cottrell, Y. Bazilevs, Isogeometric analysis: CAD, finite elements, NURBS, exact geometry and mesh refinement, Computer Methods in Applied Mechanics and Engineering 194 (39) (2005) 4135–4195.

[5] D. Schillinger, L. Dede, M. Scott, J. Evans, M. Borden, E. Rank, T. Hughes, An isogeometric design-through-analysis methodology based on adaptive hierarchical refinement of NURBS, immersed boundary methods, and T-spline CAD surfaces, Computer Methods in Applied Mechanics and Engineering 249 (2012) 116–150.

[6] E. Rank, M. Ruess, S. Kollmannsberger, D. Schillinger, A. Düster, Geometric modeling, isogeometric analysis and the finite cell method, Computer Methods in Applied Mechanics and Engineering 249 (2012) 104–115.

[7] D. Schillinger, M. Ruess, The Finite Cell Method: A review in the context of higher-order structural analysis of CAD and image-based geometric models, Archives of Computational Methods in Engineering 22 (3) (2015) 391–455.

[8] M. Ruess, D. Schillinger, Y. Bazilevs, V. Varduhn, E. Rank, Weakly enforced essential boundary conditions for NURBS-embedded and trimmed NURBS geometries on the basis of the finite cell methodod, International Journal for Numerical Methods in Engineering 95 (10) (2013) 811–846.

[9] M. Ruess, D. Schillinger, A. Özcan, E. Rank, Weak coupling for isogeometric analysis of non-matching and trimmed multi-patch geometries, Computer Methods in Applied Mechanics and Engineering 269 (2014) 46–71.

[10] Y. Guo, M. Ruess, Weak Dirichlet boundary conditions for trimmed thin isogeometric shells, Computers and Mathematics with Applications 70 (7) (2015) 1425–1440.

[11] Y. Guo, M. Ruess, D. Schillinger, A parameter-free variational coupling approach for trimmed isogeometric thin shells, Computational Mechanics 59 (4) (2017) 693–715.

[12] C. Peskin, Flow patterns around heart valves: A numerical method, Journal of Computational Physics 10 (2) (1972) 252–271.

[13] C. Peskin, Numerical analysis of blood flow in the heart, Journal of Computational Physics 25 (3) (1977) 220–252.

[14] C. Peskin, The immersed boundary method, Acta Numerica 11 (2002) 479–517.

[15] Y. Bazilevs, M.-C. Hsu, M. Scott, Isogeometric fluid–structure interaction analysis with emphasis on non-matching discretizations, and with application to wind turbines, Computer Methods in Applied Mechanics and Engineering 249 (2012) 28–41.

[16] F. Xu, D. Schillinger, D. Kamensky, V. Varduhn, C. Wang, M.-C. Hsu, The tetrahedral finite cell method for fluids: Immersogeometric analysis of turbulent flow around complex geometries, Computers and Fluids 141 (2016) 135–154.

[17] M.-C. Hsu, C. Wang, F. Xu, A. Herrema, A. Krishnamurthy, Direct immersogeometric fluid flow analysis using B-rep CAD models, Computer Aided Geometric Design 43 (2016) 143–158.

[18] E. Burman, M. Fernández, An unfitted Nitsche method for incompressible fluid–structure interaction using overlapping meshes, Computer Methods in Applied Mechanics and Engineering 279 (2014) 497–514.

[19] A. Massing, M. Larson, A. Logg, M. Rognes, A stabilized Nitsche fictitious domain method for the Stokes problem, Journal of Scientific Computing 61 (3) (2014) 604–628.

[20] Y. Wang, P. Jimack, M. Walkley, A one-field monolithic fictitious domain method for fluid–structure interactions, Computer Methods in Applied Mechanics and Engineering 317 (2017) 1146–1168.

[21] M. Wu, D. Kamensky, C. Wang, A. Herrema, F. Xu, M. Pigazzini, A. Verma, A. Marsden, Y. Bazilevs, M.-C. Hsu, Optimizing fluid–structure interaction systems with immersogeometric analysis and surrogate modeling: Application to a hydraulic arresting gear, Computer Methods in Applied Mechanics and Engineering 316 (2017) 668–693.

[22] B. Schott, W. Wall, A new face-oriented stabilized XFEM approach for 2D and 3D incompressible Navier-Stokes equations, Computer Methods in Applied Mechanics and Engineering 276 (2014) 233–265.

[23] B. Schott, S. Shahmiri, R. Kruse, W. Wall, A stabilized Nitsche-type extended embedding mesh approach for 3D low- and high-Reynolds-number flows, International Journal for Numerical Methods in Fluids 82 (6) (2016) 289–315.

[24] C. Kadapa, W. Dettmer, D. Perić, A stabilised immersed boundary method on hierarchical b-spline grids for fluid–rigid body interaction with solid–solid contact, Computer Methods in Applied Mechanics and Engineering 318 (2017) 242–269.

[25] B. Schott, U. Rasthofer, V. Gravemeier, W. Wall, A face-oriented stabilized Nitsche-type extended variational multiscale method for incompressible two-phase flow, International Journal for Numerical Methods in Engineering 104 (7) (2015) 721–748.

[26] C. Villanueva, K. Maute, CutFEM topology optimization of 3D laminar incompressible flow problems, Computer Methods in Applied Mechanics and Engineering 320 (2017) 444–473.

[27] M.-C. Hsu, D. Kamensky, Y. Bazilevs, M. Sacks, T. Hughes, Fluid–structure interaction analysis of bioprosthetic heart valves: significance of arterial wall deformation, Computational Mechanics 54 (4) (2014) 1055–1071.

[28] M.-C. Hsu, D. Kamensky, F. Xu, J. Kiendl, C. Wang, M. Wu, J. Mineroff, A. Reali, Y. Bazilevs, M. Sacks, Dynamic and fluid–structure interaction simulations of bioprosthetic heart valves using parametric design with T-splines and Fung-type material models, Computational Mechanics 55 (6) (2015) 1211–1225.

[29] E. Burman, Ghost penalty, Comptes Rendus Mathematique 348 (21) (2010) 1217–1220.

[30] R. Sanches, P. Bornemann, F. Cirak, Immersed b-spline (i-spline) finite element method for geometrically complex domains, Computer Methods in Applied Mechanics and Engineering 200 (13) (2011) 1432–1445.

[31] E. Burman, P. Hansbo, Fictitious domain finite element methods using cut elements: II. A stabilized Nitsche method, Applied Numerical Mathematics 62 (2012) 328–341.

[32] T. Rüberg, F. Cirak, A fixed-grid b-spline finite element technique for fluid–structure interaction, International Journal for Numerical Methods in Fluids 74 (9) (2014) 623–660.

[33] W. Dettmer, C. Kadapa, D. Perić, A stabilised immersed boundary method on hierarchical b-spline grids, Computer Methods in Applied Mechanics and Engineering 311 (2016) 415–437.

[34] C. Lehrenfeld, A. Reusken, Optimal preconditioners for Nitsche-XFEM discretizations of interface problems, Numerische Mathematik 135 (2) (2017) 313–332.

[35] F. de Prenter, C. Verhoosel, G. van Zwieten, E. van Brummelen, Condition number analysis and preconditioning for the finite cell method, Computer Methods in Applied Mechanics and Engineering 316 (2017) 297–327.

[36] J. Melenk, I. Babuška, The partition of unity finite element method: Basic theory and applications, Computer Methods in Applied Mechanics and Engineering 139 (1) (1996) 289–314.

[37] I. Babuška, J. Melenk, The partition of unity method, International Journal for Numerical Methods in Engineering 40 (4) (1997) 727–758.

[38] T. Belytschko, T. Black, Elastic crack growth in finite elements with minimal remeshing, International Journal for Numerical Methods in Engineering 45 (5) (1999) 601–620.

[39] N. Moës, J. Dolbow, T. Belytschko, A finite element method for crack growth without remeshing, International Journal for Numerical Methods in Engineering 46 (1) (1999) 131–150.

[40] C. Duarte, I. Babuška, J. Oden, Generalized finite element methods for three-dimensional structural mechanics problems, Computers and Structures 77 (2) (2000) 215–232.

[41] T. Strouboulis, I. Babuška, K. Copps, The design and analysis of the generalized finite element method, Computer Methods in Applied Mechanics and Engineering 181 (1) (2000) 43–69.

[42] H. Johansen, P. Colella, A Cartesian Grid Embedded Boundary Method for Poisson's Equation on Irregular Domains, Journal of Computational Physics 147 (1) (1998) 60–85.

[43] C. Lehrenfeld, M. Olshanskii, An Eulerian finite element method for PDEs in time-dependent domains, ESAIM Mathematical Modelling and Numerical Analysis 53 (2) (2019) 585–614.

[44] K. Höllig, U. Reif, J. Wipper, Weighted extended B-spline approximation of Dirichlet problems, SIAM Journal on Numerical Analysis 39 (2) (2001) 442–462.

[45] K. Höllig, C. Apprich, A. Streit, Introduction to the WEB-method and its applications, Advances in Computational Mathematics 23 (1) (2005) 215–237.

[46] T. Rüberg, F. Cirak, Subdivision-stabilised immersed b-spline finite elements for moving boundary flows, Computer Methods in Applied Mechanics and Engineering 209 (2012) 266–283.

[47] T. Rüberg, F. Cirak, J. García-Aznar, An unstructured immersed finite element method for nonlinear solid mechanics, Advanced Modeling and Simulation in Engineering Sciences 3 (1) (2016) 623–660.

[48] S. Badia, F. Verdugo, A. Martín, The aggregated unfitted finite element method for elliptic problems, Computer Methods in Applied Mechanics and Engineering 336 (2018) 533–553.

[49] S. Badia, A. Martín, F. Verdugo, Mixed Aggregated Finite Element Methods for the Unfitted Discretization of the Stokes Problem, SIAM Journal on Scientific Computing 40 (6) (2018) B1541–B1576.

[50] B. Marussig, R. Hiemstra, T. Hughes, Improved conditioning of isogeometric analysis matrices for trimmed geometries, Computer Methods in Applied Mechanics and Engineering 334 (2018) 79–110.

[51] I. Babuška, U. Banerjee, Stable generalized finite element method (SGFEM), Computer Methods in Applied Mechanics and Engineering 201 (2012) 91–111.

[52] V. Gupta, C. Duarte, I. Babuška, U. Banerjee, Stable GFEM (SGFEM): Improved conditioning and accuracy of GFEM/XFEM for three-dimensional fracture mechanics, Computer Methods in Applied Mechanics and Engineering 289 (2015) 355–386.

[53] K. Agathos, E. Chatzi, S. Bordas, Stable 3D extended finite elements with higher order enrichment for accurate non planar fracture, Computer Methods in Applied Mechanics and Engineering 306 (2016) 19–46.

[54] K. Agathos, E. Chatzi, S. Bordas, D. Talaslidis, A well-conditioned and optimally convergent XFEM for 3D linear elastic fracture, International Journal for Numerical Methods in Engineering 105 (9) (2016) 643–677.

[55] K. Agathos, G. Ventura, E. Chatzi, S. Bordas, Stable 3D XFEM/vector level sets for non-planar 3D crack propagation and comparison of enrichment schemes, International Journal for Numerical Methods in Engineering 113 (2) (2018) 252–276.

[56] S. Kleiss, C. Pechstein, B. Jüttler, S. Tomar, IETI – Isogeometric Tearing and Interconnecting, Computer Methods in Applied Mechanics and Engineering 247–248 (2012) 201–215.

[57] L. Beirão Da Veiga, D. Cho, L. Pavarino, S. Scacchi, BDDC preconditioners for isogeometric analysis, Mathematical Models and Methods in Applied Sciences 23 (6) (2013) 1099–1142.

[58] L. Beirão Da Veiga, D. Cho, L. Pavarino, S. Scacchi, Overlapping Schwarz Methods for Isogeometric Analysis, SIAM Journal on Numerical Analysis 50 (3) (2012) 1394–1416.

[59] L. Beirão Da Veiga, D. Cho, L. Pavarino, S. Scacchi, Isogeometric Schwarz preconditioners for linear elasticity systems, Computer Methods in Applied Mechanics and Engineering 253 (2013) 439–454.

[60] K. Gahalaut, J. Kraus, S. Tomar, Multigrid methods for isogeometric discretization, Computer Methods in Applied Mechanics and Engineering 253 (2013) 413–425.

[61] A. Buffa, H. Harbrecht, A. Kunoth, G. Sangalli, BPX-preconditioning for isogeometric analysis, Computer Methods in Applied Mechanics and Engineering 265 (2013) 63–70.

[62] C. Hofreither, S. Takacs, Robust Multigrid for Isogeometric Analysis Based on Stable Splittings of Spline Spaces, SIAM Journal on Numerical Analysis 55 (4) (2017) 2004–2024.

[63] S. Sangalli, M. Tani, Isogeometric preconditioners based on fast solvers for the Sylvester equation, SIAM Journal on Scientific Computing 38 (6) (2016) A3644–A3671.

[64] E. Béchet, H. Minnebo, N. Moës, B. Burgardt, Improved implementation and robustness study of the X-FEM for stress analysis around cracks, International Journal for Numerical Methods in Engineering 64 (8).

[65] A. Menk, S. Bordas, A robust preconditioning technique for the extended finite element method, International Journal for Numerical Methods in Engineering 85 (13) (2011) 1609–1632.

[66] B. Hiriyur, R. Tuminaro, H. Waisman, E. Boman, D. Keyes, A Quasi-algebraic Multigrid Approach to Fracture Problems Based on Extended Finite Elements, Siam Journal on Scientific Computing 34 (2) (2012) A603–A626.

[67] L. Berger-Vergiat, H. Waisman, B. Hiriyur, R. Tuminaro, D. Keyes, Inexact Schwarz-algebraic multigrid preconditioners for crack problems modeled by extended finite element methods, International Journal for Numerical Methods in Engineering 90 (3) (2012) 311–328.

[68] H. Waisman, L. Berger-Vergiat, An adaptive domain decomposition preconditioner for crack propagation problems modeled by XFEM, International Journal for Multiscale Computational Engineering 11 (6) (2013) 633–654.

[69] S. Badia, F. Verdugo, Robust and scalable domain decomposition solvers for unfitted finite element methods, Journal of Computational and Applied Mathematics 344 (2018) 740–759.

[70] B. Smith, P. Bjørstad, W. Gropp, Domain Decomposition: parallel multilevel methods for elliptic partial differential equations, Cambridge University Press, 1996.

[71] A. Toselli, O. Widlund, Domain Decomposition Methods: Algorithms and Theory, Springer, 2005.

[72] S. Brenner, L. Scott, The Mathematical Theory of Finite Element Methods, Springer, 2008.

[73] A. Buffa, C. de Falco, G. Sangalli, IsoGeometric Analysis: Stable elements for the 2D Stokes equation, International Journal for Numerical Methods in Fluids 65 (11–12) (2011) 1407–1422.

[74] J. Jomo, F. de Prenter, M. Elhaddad, D. D'Angella, C. Verhoosel, S. Kollmannsberger, J. Kirschke, V. Nübel, E. van Brummelen, E. Rank, Robust and parallel scalable iterative solutions for large-scale finite cell analyses, Finite Elements in Analysis and Design 163 (2019) 14–30.

[75] J. Cottrell, T. Hughes, Y. Bazilevs, Isogeometric Analysis: Toward Integration of CAD and FEA, Wiley, 2009.

[76] J. Nitsche, Über ein Variationsprinzip zur Lösung von Dirichlet-Problemen bei Verwendung von Teilräumen die keinen Randbedingungen unterworfen sind, in: Abhandlungen aus dem mathematischen Seminar der Universität Hamburg, 1971, pp. 9–15.

[77] A. Embar, J. Dolbow, I. Harari, Imposing Dirichlet boundary conditions with Nitsche's method and spline based finite elements, International Journal for Numerical Methods in Engineering 83 (7) (2010) 877–898.

[78] I. Babuška, The finite element method with penalty, Mathematics of Computation 27 (122) (1973) 221–228.

[79] E. Burman, A penalty-free nonsymmetric Nitsche-type method for the weak imposition of boundary conditions, SIAM Journal on Numerical Analysis 50 (4) (2012) 1959–1981.

[80] T. Boiveau, E. Burman, A penalty-free Nitsche method for the weak imposition of boundary conditions in compressible and incompressible elasticity, IMA Journal of Numerical Analysis 36 (2) (2016) 770–795.

[81] D. Schillinger, I. Harari, M.-C. Hsu, D. Kamensky, S. Stoter, Y. Yu, Y. Zhao, The non-symmetric Nitsche method for the parameter-free imposition of weak boundary and coupling conditions in immersed finite elements, Computer Methods in Applied Mechanics and Engineering 309 (2016) 625–652.

[82] S. Fernández-Méndez, A. Huerta, Imposing essential boundary conditions in mesh-free methods, Computational methods in applied mechanics and engineering 193 (2004) 1257–1275.

[83] J. Baiges, R. Codina, F. Henke, S. Shahmiri, W. Wall, A symmetric method for weakly imposing dirichlet boundary conditions in embedded finite element meshes, International Journal for Numerical Methods in Engineering 90 (5) (2012) 636–658.

[84] Y. Saad, Iterative Methods for Sparse Linear Systems, SIAM, 2003.

[85] M. Murphy, G. Golub, A. Wathen, A Note on Preconditioning of Indefinite Linear Systems, SIAM Journal on Scientific Computing 21 (6) (2000) 1969–1972.

[86] S. Turek, Efficient Solvers for Incompressible Flow Problems, Springer, 1999.

[87] S. Vanka, Block-implicit multigrid solution of Navier-Stokes equations in primitive variables, Journal of Computational Physics 65 (1) (1986) 138–158.

[88] A. Matsokin, S. Nepomnyaschikh, The Schwarz alternation method in a subspace, Soviet Mathematics (Izv. Vyssh. Uchebn. Zaved. Mat.) 29 (10) (1985) 78–84.

[89] P. Lions, On the Schwarz alternating method. I, in: First international symposium on domain decomposition methods for partial differential equations, 1988, pp. 1–42.

[90] X.-C. Cai, Additive Schwarz algorithms for parabolic convection-diffusion equations, Numerische Mathematik 60 (1) (1991) 41–61.

[91] X.-C. Cai, O. Widlund, Domain decomposition algorithms for indefinite elliptic problems, SIAM Journal on Scientific and Statistical Computing 13 (1) (1992) 243–258.

[92] O. Widlund, Some Schwarz methods for symmetric and nonsymmetric elliptic problems, in: Fifth International Symposium on Domain Decomposition Methods for Partial Differential Equations, 1992, pp. 19–36.

[93] X.-C. Cai, O. Widlund, Multiplicative Schwarz algorithms for some nonsymmetric and indefinite problems, SIAM Journal on Numerical Analysis 30 (4) (1993) 936–952.

[94] X.-C. Cai, W. Gropp, D. Keyes, A Comparison of Some Domain Decomposition and ILU Preconditioned Iterative Methods for Nonsymmetric Elliptic Problems, Numerical Linear Algebra with Applications 1 (5) (1994) 477–504.

[95] T. Chan, T. Mathew, Domain decomposition algorithms, Acta Numerica 3 (1994) 61–143.

[96] X.-C. Cai, C. Farhat, M. Sarkis, A Minimum Overlap Restricted Additive Schwarz Preconditioner and Applications in 3D Flow Simulations, Contemporary mathematics 218 (1998) 479–485.

[97] M. Sarkis, D. Szyld, Optimal left and right additive Schwarz preconditioning for minimal residual methods with Euclidean and energy norms, Computer Methods in Applied Mechanics and Engineering 196 (8) (2007) 1612–1621.

[98] Y. Bazilevs, C. Michler, V. Calo, T. Hughes, Isogeometric variational multiscale modeling of wall-bounded turbulent flows with weakly enforced boundary conditions on unstretched meshes, Computer Methods in Applied Mechanics and Engineering 199 (13) (2010) 780–790.

[99] J. Freund, R. Stenberg, On weakly imposed boundary conditions for second order problems, in: Proceedings of the Ninth International Conference on Finite Elements in Fluids, 1995, pp. 327–336.

[100] A. Brooks, T. Hughes, Streamline upwind/Petrov-Galerkin formulations for convection dominated flows with particular emphasis on the incompressible Navier-Stokes equations, Computer Methods in Applied Mechanics and Engineering 32 (1) (1982) 199–259.

[101] T. Hughes, L. Mazzei, K. Jansen, Large Eddy Simulation and the variational multiscale method, Computing and Visualization in Science 3 (1) (2000) 47–59.

[102] T. Hughes, G. Scovazzi, L. Franca, Multiscale and Stabilized Methods, Wiley, 2004, pp. 1–64.

[103] Y. Bazilevs, V. Calo, J. Cottrell, T. Hughes, A. Reali, G. Scovazzi, Variational multiscale residual-based turbulence modeling for large eddy simulation of incompressible flows, Computer Methods in Applied Mechanics and Engineering 197 (2007) 173–201.

[104] D. Elfverson, M. Larson, K. Larsson, CutIGA with basis function removal, Advanced Modeling and Simulation in Engineering Sciences 5 (6) (2018) 1–19.

[105] P. Wesseling, An Introduction to Multigrid Methods, Wiley, 1992.

[106] A. Brandt, O. Livne, Multigrid Techniques. 1984 Guide with Applications to Fluid Dynamics. Revised Edition, SIAM, 2011.

[107] C. Verhoosel, G. Van Zwieten, B. Van Rietbergen, R. De Borst, Image-based goal-oriented adaptive isogeometric analysis with application to the micro-mechanical modeling of trabecular bone, Computer Methods in Applied Mechanics and Engineering 284 (2015) 138–164.

[108] T. Warburton, J. Hesthaven, On the constants in hp-finite element trace inverse inequalities, Computer Methods in Applied Mechanics and Engineering 192 (25) (2003) 2765–2773.

[109] C. Johnson, Numerical Solution of Partial Differential Equations by the Finite Element Method, Cambridge University Press, 1987.

[110] K. Gahalaut, S. Tomar, Condition number estimates for matrices arising in the isogeometric discretizations, RICAM technical report 23.

[111] C.-H. Bruneau, P. Fabrie, New efficient boundary conditions for incompressible Navier-Stokes equations : a well-posedness result, ESAIM: Mathematical Modelling and Numerical Analysis 30 (7) (1996) 815–840.

[112] M. Braack, P. Mucha, Directional do-nothing condition for the Navier-Stokes equations, Journal of Computational Mathematics 32 (5) (2014) 507–521.

[113] D. Arndt, M. Braack, G. Lube, Finite Elements for the Navier-Stokes Problem with Outflow Condition, Springer, 2016, pp. 95–103.

[114] W. Layton, Introduction to the Numerical Analysis of Incompressible Flows, SIAM, 2008.

[115] Y. Bazilevs, T. Hughes, Weak imposition of Dirichlet boundary conditions in fluid mechanics, Computers and Fluids 36 (1) (2007) 12–26.

[116] T. Tezduyar, Y. Osawa, Finite element stabilization parameters computed from element matrices and vectors, Computer Methods in Applied Mechanics and Engineering 190 (3) (2000) 411–430.

[117] T. Hoang, C. Verhoosel, F. Auricchio, E. van Brummelen, A. Reali, Mixed Isogeometric Finite Cell Methods for the Stokes problem, Computer Methods in Applied Mechanics and Engineering 316 (2017) 400–423.

[118] T. Hoang, C. C.V. Verhoosel, C.-Z. Qin, F. Auricchio, A. Reali, E. van Brummelen, Skeleton-stabilized immersogeometric analysis for incompressible viscous flow problems, Computer Methods in Applied Mechanics and Engineering 344 (2019) 421–450.

[119] I.-L. Chern, Y.-C. Shu, A coupling interface method for elliptic interface problems, Journal of Computational Physics 225 (2) (2007) 2138–2174.

[120] E. Burman, M. Fernández, Continuous interior penalty finite element method for the time-dependent Navier-Stokes equations: space discretization and convergence, Numerische Mathematik 107 (1) (2007) 39–77.

[121] E. Burman, M. Fernández, Stabilization of explicit coupling in fluid–structure interaction involving fluid incompressibility, Computer Methods in Applied Mechanics and Engineering 198 (5) (2009) 766–784.

[122] G. van Zwieten, J. van Zwieten, C. Verhoosel, E. Fonn, W. Hoitinga, nutils v3.0. *https://doi.org/10.5281/zenodo.1405137*.